



Australian Government
Department of Defence
Defence Science and
Technology Organisation

Time Delay Estimation

Iain Jameson

Electronic Warfare and Radar Division
Defence Science and Technology Organisation

DSTO-TR-1705

ABSTRACT

We investigate the possibility of exploiting the properties of a detected Low Probability of Intercept (LPI) signal waveform to estimate time delay, and by geometry, angle of arrival. We consider the case where a highly correlated signal is received at two stationary passive receivers. The signal source is assumed stationary, and the signal waveform designed so that the ambiguity function has a sharp peak. We also restrict ourselves to low signal-to-noise ratios, namely 10 dB and less. We also examine the minimum time-delay estimate error – the Cramer–Rao bound.

The results indicate that the method works well for highly correlated pulsed signals, and may prove useful for other types of signals, such as CW signals and pseudo-random noise.

APPROVED FOR PUBLIC RELEASE

Published by

*Defence Science and Technology Organisation
PO Box 1500
Edinburgh, South Australia 5111, Australia*

*Telephone: (08) 8259 5555
Facsimile: (08) 8259 6567*

*© Commonwealth of Australia 2006
AR-013-376*

APPROVED FOR PUBLIC RELEASE

Time Delay Estimation

EXECUTIVE SUMMARY

The theory of radar signal (target echo) detection can be formulated with the use of the ambiguity function. Such functions are designed to have sharp peaks, and a high correlation on return. Resolution is determined by the width of the peak.

To improve detection and target resolution such signals make use of pulse compression techniques.

An Electronic Support measures (ESM) system can exploit this information by using two passive receivers, separated in space. Knowing the received waveform will have a sharply peaked ambiguity function, we look at the correlation between the output of one receiver, with the output of the second.

This correlation will give us the time-delay, to the same resolution as was “built into” the original waveform. From this, using simple geometry, the signals angle of arrival can be determined.

Waveform design is performed in the frequency domain, making use of complex signals. As a result, we work primarily within the frequency domain.

The starting point is the analytic signal. We generate such a signal, and form the product of the signal with its (complex conjugate) time-delayed version. This product, in the frequency domain, is the cross spectral density. Transforming to the time domain, we find the peak of the time-domain correlation function, using quadratic interpolation.

This peak gives the estimate of the time-delay.

We have run simulations over various signal-to-noise ratios (SNRs) with continuous wave and single pulse chirped signals. As we are interested in the ability to estimate time-delay at low SNR, we run our simulations with SNR at 10 dB and less.

The continuous wave case allows us to observe the effects of frequency wrap around, as the waveform will resemble a partial sawtooth during the sample time.

The continuous wave simulations show that there is a bias due to the frequency wrap around, producing a rough measure of the actual time-delay. The single pulse case gives very good estimates of the time delay, although all estimates degrade as the SNR decreases.

We have also tested the algorithm on pseudo-random noise generated during the Electronic Warfare and Radar Division (EWRD) Durex trial. Again, although we do not accurately estimate time-delay, we do get a rough measure of the delay.

The results indicate that the method works well for highly correlated pulsed signals, and may prove useful for other types of signals, such as CW signals and pseudo-random noise.

Author

Iain Jameson
Electronic Warfare and Radar Division

Iain Jameson was first employed by the Electronic Warfare Division, SAP group, in May 1996. He has a Ph.D. in Theoretical Physics from the University of Adelaide.

Contents

1	Introduction	1
2	Time-Delay Estimation	2
2.1	Introduction	2
2.2	Cramer-Rao Bound for a Single Pulse	4
2.3	Estimation	5
2.3.1	Continuous-Wave Cramer-Rao Bound	8
2.3.2	Simulations	11
2.3.2.1	Continuous Wave	11
2.3.2.2	Single Pulse	24
3	EWRD Durex Trial Data	33
4	Time-Domain Filtered Cross Spectral Density	37
5	Discussion	38
6	Acknowledgments	40
References		41

Appendices

A	Optimum Passive Bearing Estimation	43
A.1	Cramer-Rao Bound	43
B	Generalised Cross Correlation Method	47

Figures

1	Quadratic Interpolation	6
2	Geometry of receiver system	11
3	Instantaneous frequency of chirp waveform over sample time	12
4	Cross Spectral Density – CW	13
5	Time-delay estimate. $L = 10$ m, $t_d = 5.8$ n sec, CW	15
6	Angle estimate. $L = 10$ m, $\theta = 10^\circ$, CW	15

7	Time-delay estimate. $L = 10$ m, $t_d = 16.7$ n sec, CW	16
8	Angle estimate. $L = 10$ m, $\theta = 30^\circ$, CW	16
9	Time-delay estimate. $L = 10$ m, $t_d = 32.8$ n sec, CW	17
10	Angle estimate. $L = 10$ m, $\theta = 80^\circ$, CW	17
11	Time-delay estimate. $L = 30$ m, $t_d = 17.4$ n sec, CW	19
12	Angle estimate. $L = 30$ m, $\theta = 10^\circ$, CW	19
13	Time-delay estimate. $L = 30$ m, $t_d = 70.7$ n sec, CW	20
14	Angle estimate. $L = 30$ m, $\theta = 45^\circ$, CW	20
15	Time-delay estimate. $L = 30$ m, $t_d = 94$ n sec, CW	21
16	Angle estimate. $L = 30$ m, $\theta = 70^\circ$, CW	21
17	Variance versus SNR. $L = 10$ m, $\theta = 30^\circ$	22
18	Variance versus SNR. $L = 10$ m, $\theta = 10^\circ$, CW	23
19	Instantaneous frequency of chirp waveform over sample time – single pulse	24
20	Cross Spectral Density – single pulse	25
21	Time-delay estimate, $L = 10$ m, $t_d = 5.8$ ns, single pulse	26
22	Angle estimate, $L = 10$ m, $\theta = 10^\circ$, single pulse	26
23	Time-delay estimate, $L = 10$ m, $t_d = 16.7$ ns, single pulse	27
24	Angle estimate, $L = 10$ m, $\theta = 30^\circ$, single pulse	27
25	Time-delay estimate, $L = 10$ m, $t_d = 32.8$ ns, single pulse	28
26	Angle estimate, $L = 10$ m, $\theta = 80^\circ$, single pulse	28
27	Time-delay estimate, $L = 30$ m, $t_d = 17.4$ ns, single pulse	29
28	Angle estimate, $L = 30$ m, $\theta = 10^\circ$, single pulse	29
29	Time-delay estimate, $L = 30$ m, $t_d = 70.7$ ns, single pulse	30
30	Angle estimate, $L = 30$ m, $\theta = 45^\circ$, single pulse	30
31	Time-delay estimate, $L = 30$ m, $t_d = 94$ ns, single pulse	31
32	Angle estimate, $L = 30$ m, $\theta = 70^\circ$, single pulse	31
33	Time-delay as a function of angle	33
34	Receiver – Transmitter geometry, Durex trial	34
35	Durex trial, time-delay versus angle.	36

Tables

3.1	Angle estimates from Durex trial data	35
3.2	Time-delay estimates from Durex trial data	35

1 Introduction

The ability to find the direction of an emitted signal is of importance in a wide range of fields, including electronic intelligence (ELINT) and electronic warfare support (ES).

For a digital receiver, direction finding is necessarily preceded by signal detection, and parameter estimation, and this leads to the theory of waveform design. In developing the theory of waveform design and analysis, it is found that a simplification of the analysis can be achieved by working in the complex domain, and by generalising the phasor description of signals [2]. As a result, it is sensible to work in the frequency domain, returning to the time domain as needed.

For ranging, an emitted waveform is correlated with the return from a target. As the waveform used is designed to be highly correlated – its ambiguity function will have a sharp peak – there will be a sharp peak in the correlation function. This peak gives the time–delay, or range of the target.

An electronic support measures (ESM) system can exploit this information, and use it to determine the direction of the signal source. We do this by correlating the received signal in a passive receiver, with the time–delayed signal in a second passive receiver, located a short distance away in space. The output of this correlator receiver is the time–delay, and by geometry, the angle of arrival.

This is shown in Chapter 2. We start by introducing the ambiguity function, and the method used for estimating the time–delay. We run simulations over various Signal–to–Noise ratios (SNR), for both continuous wave (CW), and single–pulse signals. In this chapter we also derive expressions for the Cramer–Rao bound of the variance of the estimates.

In Chapter 3 we apply the techniques developed in Chapter 2 to pseudo–random noise, generated at the Electronic Warfare and Radar Division (EWRD) Durex trial [1].

In Chapter 4, we briefly review a technique which uses the phase slope of the cross spectral density to estimate time delay. In this way, we see that it is not necessary to transform back to the time–domain in order to estimate the time–delay.

In Appendix A we review an alternative method for deriving the Cramer–Rao bound for the estimate of angle of arrival, and review the generalisation of this method in Appendix B.

2 Time-Delay Estimation

2.1 Introduction

Suppose our aim is to distinguish different ranges (time-delays) at a receiver. The transmitted signal waveform must have the property that it is as different from its shifted self as possible [3].

That is, if $\psi(t)$ represents our complex transmitted waveform, then the mean square difference [4]

$$\int |\psi(t) - \psi(t + \tau)|^2 dt \quad (1)$$

must be as large as possible over the time range containing the delay τ .

This excludes a small range of τ near zero, where $\psi(t)$ must resemble $\psi(t + \tau)$.

Expanding the term inside the integral, for complex waveforms, we find that we need to minimise (except near $\tau = 0$)

$$\Re \int \psi(t) \psi^*(t + \tau) dt \quad (2)$$

with \Re denoting the real part of the integral, and $*$ denoting complex conjugation.

We see this by considering $\psi(t)$ and $\psi(t + \tau)$ as complex vectors, with the same origin. We keep $\psi(t)$ fixed, and rotate $\psi(t + \tau)$ until the vector connecting their end points, $|\psi(t) - \psi(t + \tau)|$, is maximised.

If we write

$$\psi(t) = u(t) e^{i\omega t} \quad (3)$$

then we minimise

$$\Re e^{-i\omega\tau} \int u(t) u^*(t + \tau) dt \quad (4)$$

an oscillatory function of τ . That is, if this becomes negative for a particular value of τ , then there will be a corresponding positive value close to it. Thus we make the modulus as small as possible.

That is, we minimise the modulus of

$$c(\tau) = \int u(t) u^*(t + \tau) dt \quad (5)$$

which is the complex auto-correlation function.

We choose $u(t)$ such that $|c(\tau)| \approx 0$ except at $\tau = 0$, where it is a maximum. Note that, if $|c(\tau)| = 0$ except at $\tau = 0$, we avoid range ambiguities.

Range accuracy for a stationary target depends only upon the energy of the signal and the bandwidth of the signal energy spectrum, denoted by β [4].

For a single target, the accuracy with which τ can be determined is limited only by the amount of noise present. If $u(t)$ and $u(t + \tau)$ differ, the difference can be observed if noise is small enough.

Accuracy of measurement depends only on SNR (assumed large) and the properties of $c(\tau)$ near $\tau = 0$. A Taylor expansion gives the parabola

$$c(\tau) \approx a - b\tau^2 \quad (6)$$

where a and b are constants, and accuracy is found to be [4]

$$\delta\tau = \frac{1}{\beta\sqrt{\text{SNR}}} \quad (7)$$

where, for a pulsed radar, $1/\beta \propto$ pulse length.

The above is for a stationary target.

We now consider a moving target. Theoretically, there is no limitation on the accuracy of range or velocity (frequency), given a broad spectrum (for range) and a long time duration waveform (for velocity).

However, there are accuracy limitations on the combined resolution in time and frequency.

For targets at different ranges and velocities, neither of which is known, we require a correlation function for a combined time and frequency shift. This is

$$\chi(\tau, \phi) = \int u(t) u^*(t + \tau) e^{-i2\pi\phi t} dt \quad (8)$$

with normalisation

$$\chi(0, 0) = 1 \quad (9)$$

The interpretation is that a target with range and velocity (τ_0, ϕ_0) cannot be distinguished from a target shifted in time and frequency at $(\tau_0 + \tau, \phi_0 + \phi)$ if $\chi(\tau, \phi) = 1$ (complete ambiguity).

That is, if the ambiguity function has a sharp peak at the origin, and no other ‘large’ peaks, then the waveform has good simultaneous range and velocity resolution.

Resolving a pair of targets is not as straight forward. We can no longer expand $c(\tau)$, or more generally $\chi(\tau, \phi)$, as a parabola, as the sum of two parabolic functions is another parabolic function, with a single peak. Thus it will look like we have a single target.

This means the first two terms of the Taylor expansion say nothing about the resolving power of the waveform.

Including higher order terms, we have [5]

$$|\chi(\tau, \phi)| = \chi(0, 0) \left[1 - \frac{1}{2} (\beta^2 \tau^2 + 2A_{12}\tau\phi + \alpha^2 \phi^2 + \dots) \right] \quad (10)$$

with β the effective bandwidth of the signal when the mean frequency is zero, α is the effective duration of the signal when the mean time is zero, and A_{12} is a range-doppler coupling term [6, 7].

2.2 Cramer–Rao Bound for a Single Pulse

Similar to Equation (6), we have now the uncertainty ellipse, and the width of this ellipse in the range and velocity directions is [7]

$$\delta\tau = \frac{1}{\beta\sqrt{\text{SNR}}} \quad (11)$$

$$\delta\phi = \frac{1}{\alpha\sqrt{\text{SNR}}} \quad (12)$$

The aim is to estimate time–delay and doppler. As we want our estimates to be as accurate as possible, we want the error measurements to be as small as possible – this is the error variance, and the minimum error variance is the Cramer–Rao bound. That is, our estimate will be the actual value of the time–delay or doppler, plus/minus an error. We wish to minimise the variance of this error.

It is found that the minimum error variance is

$$E[(\hat{\tau} - \tau)^2] = \frac{1}{\beta^2 \text{SNR}} \quad (13)$$

$$E[(\hat{\phi} - \phi)^2] = \frac{1}{\alpha^2 \text{SNR}} \quad (14)$$

with $\hat{\tau}$ and $\hat{\phi}$ representing the estimate of the time–delay, and doppler, respectively.

In the above the SNR refers to the input SNR. Defining $\text{SNR}_e = BT \times (\text{SNR})$ to be the effective output SNR, where B is the noise bandwidth and T the pulse duration, then we can write [8]

$$E[(\hat{\tau} - \tau)^2] = \frac{1}{\beta^2 \text{SNR}_e} \quad (15)$$

$$E[(\hat{\phi} - \phi)^2] = \frac{1}{\alpha^2 \text{SNR}_e} \quad (16)$$

For a single pulse, the noise bandwidth is the inverse of the sample rate (half the Nyquist rate).

In order to distinguish signals at different ranges, we need to make $|\chi(\tau, 0)|$ as small as possible everywhere, except at $\tau = 0$.

Measurement accuracy usually assumes that one signal is present, and depends on the signal-to-noise ratio and the behaviour of $|\chi(\tau, \phi)|$ in a small region about $\tau = 0$ and $\phi = 0$.

The minimum error variances given above require a knowledge of α and β . For a single linear FM pulse, frequency ranging over an interval Δf , with rectangular envelope [7],

$$\alpha^2 = \frac{\pi^2 T^2}{3} \quad (17)$$

$$\beta^2 = \frac{\pi^2 (\Delta f)^2}{3} \quad (18)$$

$$A_{12} = \frac{\pi^2 T \Delta f}{3} \quad (19)$$

2.3 Estimation

We now consider the case of a stationary ESM system. A waveform has been emitted, designed to have a sharply peaked ambiguity function. As a result, the target echo will be highly correlated to the original signal. The resolution is determined by the width of the peak.

We can exploit this knowledge, and determine angle of arrival, by using two passive receivers, separated in space. Knowing the signal is highly correlated, we simply correlate the output of one of the receivers with the time-delayed output of the other. This will give us the time-delay, and hence, by geometry, the angle of arrival.

As it is usual, in waveform design, to work in the frequency domain, we do so here. When it is time to estimate the time-delay, we will perform an inverse Fourier transform, and move into the time-domain.

The algorithm proceeds as follows.

Step 1: We have real data from two receivers, $x_A(t)$ from receiver 1, and $x_B(t)$ from receiver 2 – two time series. The receivers are assumed to be stationary, and separated in space.

Step 2: We obtain the signal spectrum via a Discrete-time Fourier Transform, denoted $X_A(f)$ and $X_B(f)$.

At this point we are faced with the problem of redundancy. The original series was real, and therefore should only contain positive frequencies. Under a Fourier transform, we have generated a complex function with positive and negative frequencies. Before we can continue, we must suppress the negative frequencies [5, 6, 9].

It can be shown that if a complex signal can be written as the sum of a real part, and an imaginary part, and if these parts are related by a Hilbert transform, then one half of the spectrum will be suppressed [2].

A signal satisfying the above is called an analytic signal.

Step 3: Create signals with no negative frequencies.

Let $\psi(t)$ denote the analytic signal.

The frequency spectrum of $\psi(t)$ is [2, 5, 6]

$$\begin{aligned}\Psi(f) &= 2 X(f) & f > 0 \\ &= 0 & \text{otherwise}\end{aligned}$$

Thus, having obtained the signal spectrum in Step 2, we simply double the amplitude for positive frequencies, and set all other amplitudes to zero.

Step 4: The zero doppler Ambiguity function reduces to a complex cross correlation, in the time domain. In the frequency domain, it is the product of the Fourier transforms $\Psi_A(f)$ and $\Psi_B^*(f)$.

Thus, we calculate $\Psi_A(f) \Psi_B^*(f)$ - the Cross Spectral density.

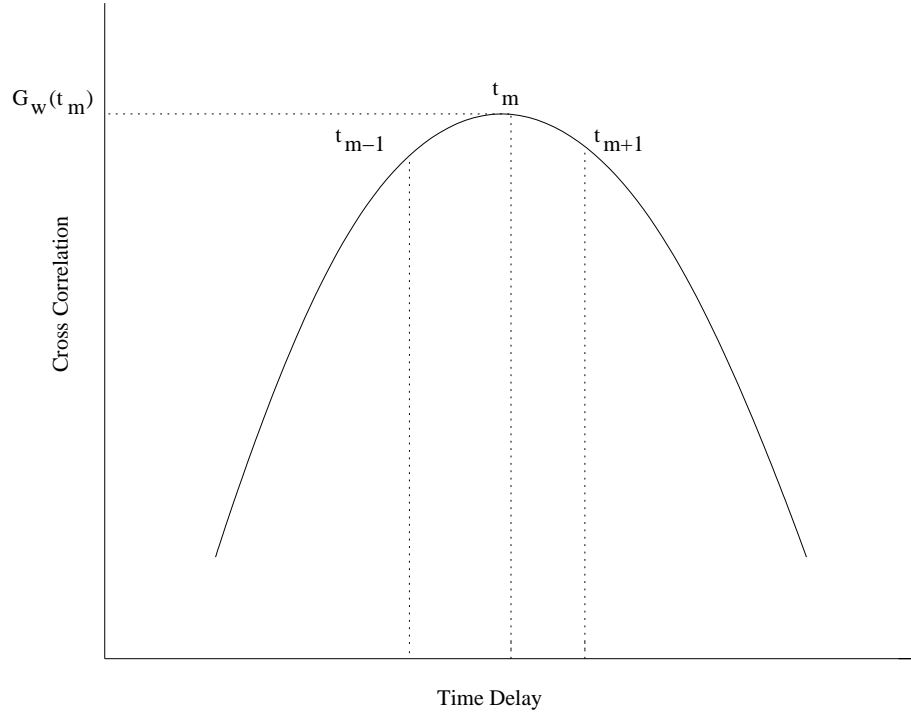


Figure 1: Quadratic Interpolation

Step 5: We revert back to the time domain via an inverse Fourier transform of the power Spectral density, in order to produce the CCF. We zero pad the IFFT in order to interpolate the CCF.

Zero padding involves interpolation by increasing sample rate. To increase the sample rate by the factor k , we need to calculate $k - 1$ intermediate values within the original time series [10].

Zero padding not only increases the number of points in our new time series, but it changes the sample rate. If the original time series has N data points, and if the zero padding factor is k , then the new time series will have kN data points. If the original time series was sampled every T seconds, then the new time series will be sampled every T/k seconds.

If we assume the signal is a stationary process, then we would expect a single peak at the value of the time-delay. As a result, we could expect the correlation function to be approximated by a parabola near the peak. The peak of this parabola is found by parabolic interpolation – we use three points, one on either side of the local maxima (as shown in Figure 1), to find the peak, and estimate the time-delay [11, 12, 13].

Using Newton's 'forward interpolation method', we Taylor expand the cross correlation function about the local maxima t_m

$$G_w(t) = |G_w(t_m)| + (t - t_m) \frac{\Delta G_0}{h} + \frac{1}{2}(t - t_m)(t - t_{m-1}) \frac{\Delta^2 G_0}{h^2} \quad (20)$$

where

$$\Delta G_0 = |G_w(t_m)| - |G_w(t_{m-1})| \quad (21)$$

and

$$\Delta^2 G_0 = |G_w(t_{m+1})| - 2|G_w(t_m)| + |G_w(t_{m-1})| \quad (22)$$

with $h = t_m - t_{m-1}$.

Expanding out the factors in the Taylor expansion gives

$$G_w(t) = c + t \left(\frac{\Delta G_0}{h} - \frac{1}{2h^2}[t_{m-1} + t_m]\Delta^2 G_0 \right) + \frac{1}{2h^2}t^2\Delta^2 G_0 \quad (23)$$

where c is a constant.

We see that if we write $-h = t_{m-1} - t_m$, then

$$t_{m-1} + t_m = -(h - 2t_m) \quad (24)$$

and we can write

$$G_w(t) = c + t \left(\frac{\Delta G_0}{h} + \frac{1}{2h^2}[h - 2t_m]\Delta^2 G_0 \right) + \frac{1}{2h^2}t^2\Delta^2 G_0 \quad (25)$$

If we define

$$a = \frac{1}{2h^2}\Delta^2 G_0 \quad (26)$$

$$b = \frac{\Delta G_0}{h} + a[h - 2t_m] \quad (27)$$

then

$$G_w(t) = a t^2 + b t + c \quad (28)$$

with maxima at the zero of the derivative with respect to the time-delay.

That is, the estimate of the time-delay, using quadratic interpolation, is

$$\begin{aligned} \hat{t}_d &= -\frac{b}{2a} \\ &= t_m + t_{m-1} - h \frac{|G_w(t_m)| - |G_w(t_{m-1})|}{|G_w(t_{m+1})| - 2|G_w(t_m)| + |G_w(t_{m-1})|} \end{aligned} \quad (29)$$

after substituting for a and b .

Substituting this back into the above quadratic, gives the value of G_w at the maxima,

$$G_0 \equiv G_w(\hat{t}_d) = -\frac{b^2}{4a} + c \quad (30)$$

The constant c can be written in terms of a and b ,

$$c = |G_w(t_m)| - b t_m - a t_m^2 \quad (31)$$

by collecting the terms not shown explicitly in Equation (23) and using Equation (24).

A property of the ambiguity function is that its maximum occurs at the origin, and is given by [5]

$$|\chi(\tau, \phi)| \leq \chi(0, 0) = 2E \quad (32)$$

with E the signals energy. Thus, given Equation (30), we can find E .

From the Taylor expansion of the ambiguity function, we see that the effective bandwidth is

$$\beta^2 = \frac{-1}{|\chi(0,0)|} \frac{\partial^2 G_w(t)}{\partial t^2} \quad (33)$$

evaluated at \hat{t}_d . That is,

$$\beta^2 = -\frac{2a}{G_0} \quad (34)$$

and reflects the curvature of the ambiguity function, at the peak.

In terms of the effective bandwidth, or curvature, we have, from Equation (29)

$$\hat{t}_d = \frac{b}{\beta^2 G_0} \quad (35)$$

and so, for fixed G_0 , the time-delay estimate depends on the curvature of the ambiguity function (at its peak). The greater the curvature, the narrower the ambiguity function at the peak, leading to an improved estimate of the time-delay.

We see from the definition of β^2 given by Equation (18), that by increasing the effective bandwidth, we increase Δf , and as a result, we increase chirp rate (if nothing else changes).

Thus the curvature of the ambiguity function at its peak depends on the chirp rate – the greater the chirp rate, the narrower the peak.

2.3.1 Continuous-Wave Cramer–Rao Bound

The Continuous-wave Cramer–Rao bound (CW CR-bound) can be found from the log likelihood function of the “system” under consideration.

For example, we consider a quadrature signal at one receiver, and its time-delayed form received at a second receiver. Assuming the same signal amplitude at both receivers, the signal functions are

$$\begin{aligned} s_1(t_n) &= b \cos[2\pi f_b t_n + \pi \alpha t_n^2] + i b \sin[2\pi f_b t_n + \pi \alpha t_n^2] \\ s_2(t_n) &= b \cos[2\pi f_b(t_n - t_d) + \pi \alpha(t_n - t_d)^2] + i b \sin[2\pi f_b(t_n - t_d) + \pi \alpha(t_n - t_d)^2] \end{aligned} \quad (36)$$

where s_1 refers to the signal in receiver 1, and s_2 refers to the signal in receiver 2. We also define f_b to be the initial chirp frequency, and chirp

$$\alpha = \frac{f_e - f_b}{\Delta t} \quad (37)$$

with f_e the end chirp frequency, and Δt the time it takes to increase (or decrease) from f_b to f_e .

For receiver 1, define

$$\begin{aligned} X_1(t_n) &= \Re[s_1(t_n)] + W(t_n) \\ Y_1(t_n) &= \Im[s_1(t_n)] + \check{W}(t_n) \\ Z_1(t_n) &= X_1(t_n) + i Y_1(t_n) \end{aligned} \quad (38)$$

with $W \sim N(0, \sigma^2)$, so

$$\begin{aligned} X_1(t_n) &\sim N(b \cos[2\pi f_b t_n + \pi \alpha t_n^2], \sigma^2) \equiv N(\mu_1(n), \sigma^2) \\ Y_1(t_n) &\sim N(b \sin[2\pi f_b t_n + \pi \alpha t_n^2], \sigma^2) \equiv N(\nu_1(n), \sigma^2) \end{aligned} \quad (39)$$

having defined $\mu_1(n) = b \cos[2\pi f_b t_n + \pi \alpha t_n^2]$ and $\nu_1(n) = b \sin[2\pi f_b t_n + \pi \alpha t_n^2]$.

The pdf of Z_1 can be written

$$p(Z_1) = \frac{1}{(2\pi\sigma^2)^N} e^{-\frac{1}{2\sigma^2} \sum_{n=0}^{N-1} ([X_1(t_n) - \mu_1(n)]^2 + [Y_1(t_n) - \nu_1(n)]^2)} \quad (40)$$

Similarly, for receiver 2, define

$$\begin{aligned} X_2(t_n) &= \Re[s_2(t_n)] + W(t_n) \\ Y_2(t_n) &= \Im[s_2(t_n)] + \check{W}(t_n) \\ Z_2(t_n) &= X_2(t_n) + i Y_2(t_n) \end{aligned} \quad (41)$$

so that

$$\begin{aligned} X_2(t_n) &\sim N(b \cos[2\pi f_b(t_n - t_d) + \pi \alpha(t_n - t_d)^2], \sigma^2) \equiv N(\mu_2(n), \sigma^2) \\ Y_2(t_n) &\sim N(b \sin[2\pi f_b(t_n - t_d) + \pi \alpha(t_n - t_d)^2], \sigma^2) \equiv N(\nu_2(n), \sigma^2) \end{aligned} \quad (42)$$

defining $\mu_2(n) = b \cos[2\pi f_b(t_n - t_d) + \pi \alpha(t_n - t_d)^2]$ and $\nu_2(n) = b \sin[2\pi f_b(t_n - t_d) + \pi \alpha(t_n - t_d)^2]$.

The pdf of Z_2 can be written

$$p(Z_2) = \frac{1}{(2\pi\sigma^2)^N} e^{-\frac{1}{2\sigma^2} \sum_{n=0}^{N-1} ([X_2(t_n) - \mu_2(n)]^2 + [Y_2(t_n) - \nu_2(n)]^2)} \quad (43)$$

Finally, define the vector

$$Z(t_n) = [Z_1(t_n) \ Z_2(t_n)]^T \quad (44)$$

then

$$f(Z) = \frac{1}{(2\pi\sigma^2)^{2N}} e^{-\frac{1}{2\sigma^2} \sum_{n=0}^{N-1} ([X_1(t_n) - \mu_1(n)]^2 + [Y_1(t_n) - \nu_1(n)]^2 + [X_2(t_n) - \mu_2(n)]^2 + [Y_2(t_n) - \nu_2(n)]^2)} \quad (45)$$

The Cramer–Rao bound is obtained from the Fisher information matrix [14]

$$J_{ij} = E \left[\frac{\partial \ln f(Z)}{\partial \alpha_i} \frac{\partial \ln f(Z)}{\partial \alpha_j} \right] \quad (46)$$

with $1 \leq i, j \leq k$, for k parameters. In the CW case, the α_i are elements of the set (f_b, b, τ, α) , so $k = 4$. The symbol E in the above Equation represents the expectation.

Performing the differentiation, and expanding, we find that

$$\begin{aligned} J_{ij} &= \frac{1}{\sigma^2} \sum_{n=0}^{N-1} \left[\frac{\partial \mu_1(n)}{\partial \chi_i} \frac{\partial \mu_1(n)}{\partial \chi_j} + \frac{\partial \mu_2(n)}{\partial \chi_i} \frac{\partial \mu_2(n)}{\partial \chi_j} + \frac{\partial \nu_1(n)}{\partial \chi_i} \frac{\partial \nu_1(n)}{\partial \chi_j} + \frac{\partial \nu_2(n)}{\partial \chi_i} \frac{\partial \nu_2(n)}{\partial \chi_j} \right. \\ &\quad + r_X \left(\frac{\partial \mu_1(n)}{\partial \chi_i} \frac{\partial \mu_2(n)}{\partial \chi_j} + \frac{\partial \mu_2(n)}{\partial \chi_i} \frac{\partial \mu_1(n)}{\partial \chi_j} \right) \\ &\quad \left. + r_Y \left(\frac{\partial \nu_1(n)}{\partial \chi_i} \frac{\partial \nu_2(n)}{\partial \chi_j} + \frac{\partial \nu_2(n)}{\partial \chi_i} \frac{\partial \nu_1(n)}{\partial \chi_j} \right) \right] \quad 1 \leq i, j \leq 4 \end{aligned} \quad (47)$$

for the Fisher information matrix, with $\chi_1 = f_b$, $\chi_2 = b$, $\chi_3 = t_d$ and $\chi_4 = \alpha$.

A consequence of the signal model we have chosen is that there will be cross terms in the Fisher information matrix. In the above, r_X and r_Y are the correlation coefficients for X and Y . That is,

$$r_X = \frac{\text{cov}(X_1, X_2)}{\sqrt{\text{var}(X_1)\text{var}(X_2)}} \quad (48)$$

with $-1 \leq r_X \leq 1$. Similarly for r_Y .

In what is to follow, rather than calculate the correlation coefficients, we consider two special cases: $r_X = r_Y = 1$ for high SNR, when we can expect some correlation, and $r_X = r_Y = 0$ for low SNR, and little correlation. We justify this by considering the number of data samples receiver 2 lags behind receiver 1. For small time-delays, up to 20 ns, say, receiver 2 will only be a few samples behind receiver 1 (eg, sampling at 5 ns). For high SNR, we can expect the waveform in receiver 2 to follow that in receiver 1, except near the peaks and troughs for sinusoids, and the beginning and end of the frequency ramp for chirped signals. For low SNR, we can not expect this.

A consequence of the non-linear time terms in the signal model is that the calculation of this matrix, and the inverse, becomes quite complicated. For the case where there is no chirp (the three dimensional case), we obtain expressions for the variance of \hat{f} and \hat{b} which are similar (up to a factor) to those found by Rife and Boornstyn [14]. The variances are smaller by a factor of 4, due to the fact we are considering the two receiver case. The variance of \hat{t}_d shows it depends explicitly on \hat{f} (again we are only considering the two cases of $r_X = r_Y = 1$ and $r_X = r_Y = 0$).

The four dimensional case shows that the variances of the parameters under consideration are dependent on the estimates of those parameters.

For example, at high SNR ($r_X = r_Y = 1$),

$$J_{33} = \left(\frac{2\pi b}{\sigma} \right)^2 \sum_{n=0}^{N-1} [\hat{f}_b + \hat{\alpha}(t_n - \hat{t}_d)^2] \quad (49)$$

which we see is a function of \hat{t}_d , the estimate of the time-delay.

For the case where f_b , b and α are known, the Cramer–Rao bound for the variance of the time-delay would simply be the inverse of J_{33} . For the case where they are all unknown, the variance will be a function of J_{33} .

We should point out that this dependence is not entirely unexpected. Rife and Boornstyn derive expressions for the variance of frequency and phase, both of which show amplitude dependence [14].

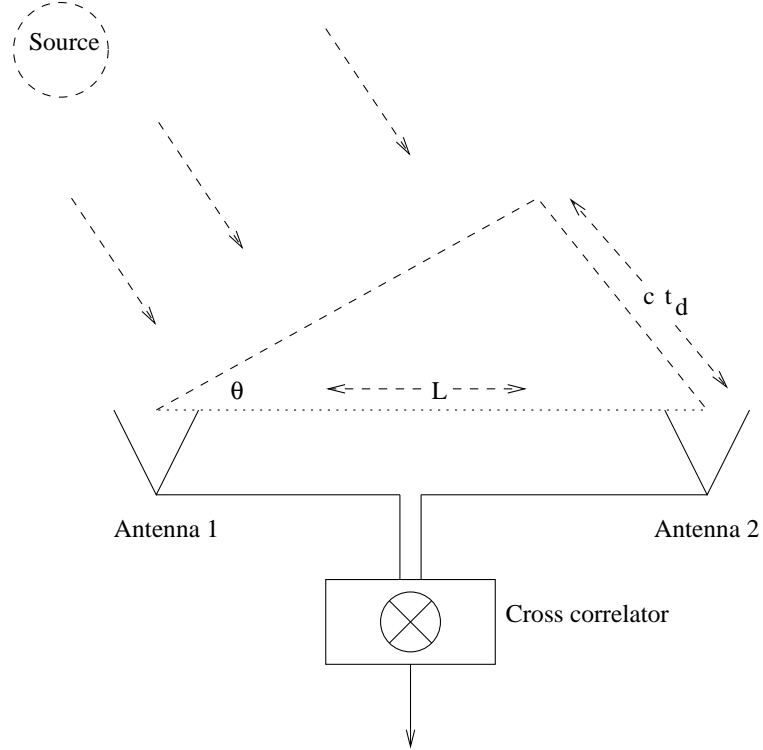


Figure 2: Geometry of receiver system

2.3.2 Simulations

2.3.2.1 Continuous Wave

The algorithm described above has been coded in Matlab. A continuous wave (CW) signal is linearly swept from $f_b = 5$ MHz to $f_e = 35$ MHz, over $\Delta t = 1$ millisecond, to produce a sawtooth waveform over the sample time. This sawtooth waveform will allow us to observe the effects of frequency wrap around on our estimates.

Figure 2 shows the geometry of the receiver. From this we have the time-delay

$$t_d = \frac{L}{c} \sin \theta \quad (50)$$

where c is the speed of light, and θ is the angle of arrival.

We show the instantaneous frequency in Figure 3, plotted using the Matlab specgram function [15].

The instantaneous frequency is proportional to the time derivative of the phase of the signal. Namely,

$$f_I = \frac{1}{2\pi} \frac{\partial \phi}{\partial t} \quad (51)$$

with

$$\phi = 2\pi(f t + \alpha t^2/2) \quad (52)$$

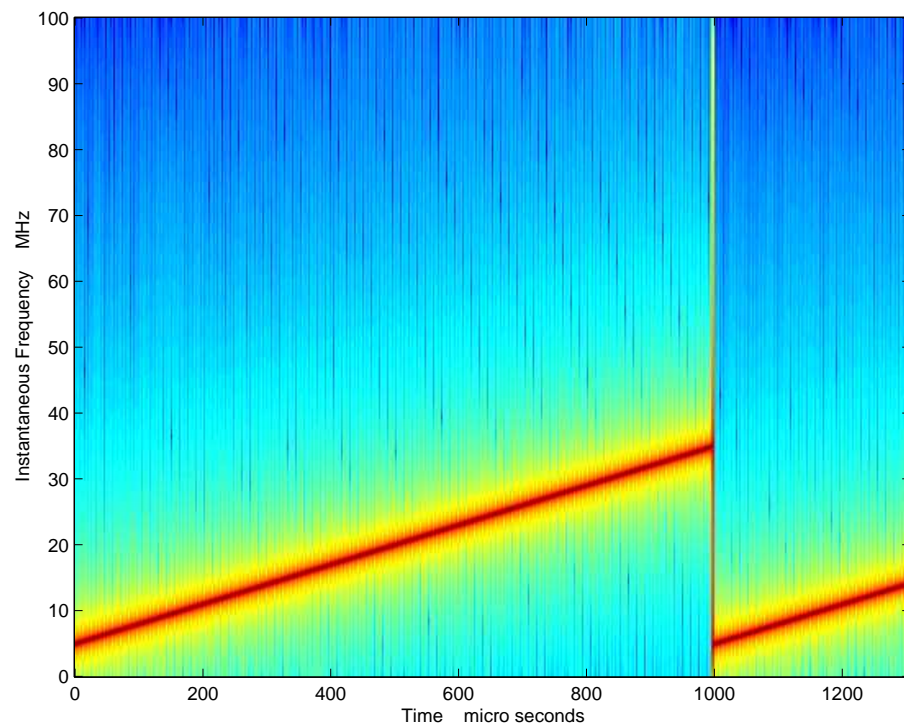


Figure 3: Instantaneous frequency of chirp waveform over sample time

An example of the cross spectral density is shown in Figure 4. It shows clearly the effect of noise and the sawtooth shape of the instantaneous frequency. In this Figure, SNR is 10 dB.

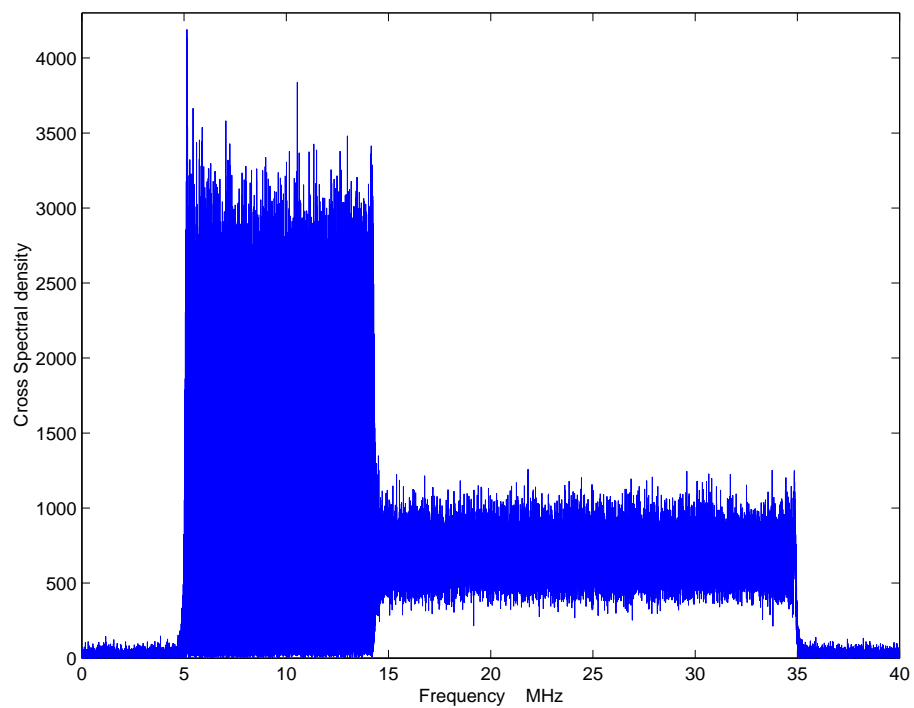


Figure 4: Cross Spectral Density – CW

In Figures 5 to 16 we plot histograms of the estimate of the time-delay. The simulation used to estimate the time-delay ran over 1024 iterations, with 2^{18} data points, and a sample rate of 5 ns. This number of points is used for simulation purposes only.

Although this report is mainly concerned with time-delay estimation, angle estimation will be required when we come to the EWRD Durex trial data. As such, we also give angle estimates in the following figures. Angle estimates are obtained from the time-delay estimate after each iteration, by inverting Equation (50), and replacing t_d with \hat{t}_d .

In Figures 5 to 10, we fix the antenna separation at $L = 10$ m, and vary θ and SNR. In Figures 11 to 16, we fix the antenna separation at $L = 30$ m, and vary θ and SNR. We use different true time-delays for both separations in order to consider a wide range of values.

The estimate of the time-delay was taken to be the value with the maximum count number in the histogram. This value was then used in the estimate of the angle of arrival.

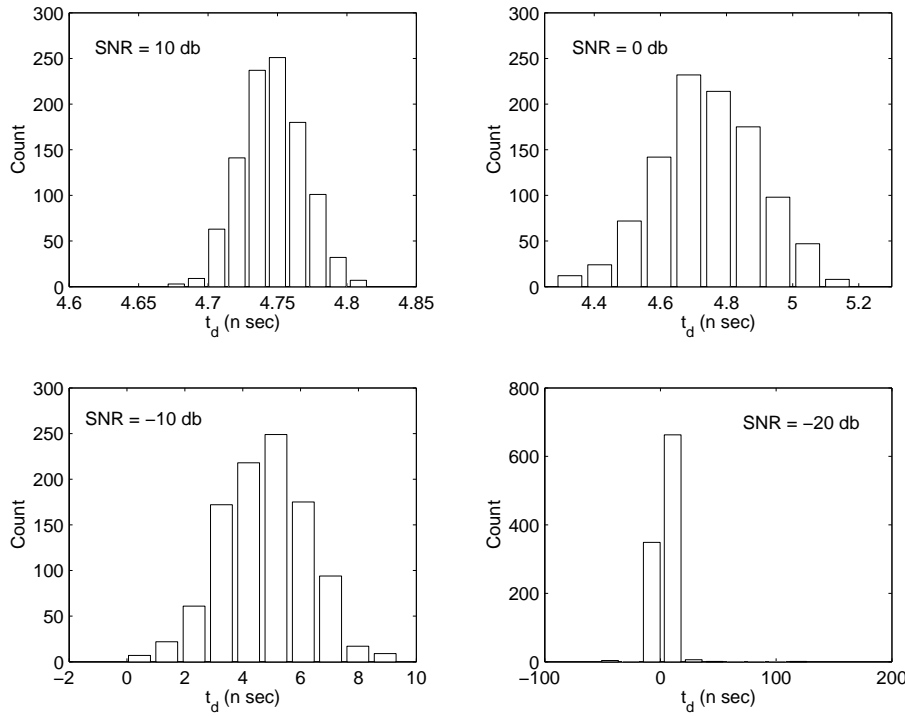


Figure 5: Time-delay estimate. $L = 10$ m, $t_d = 5.8$ n sec, CW

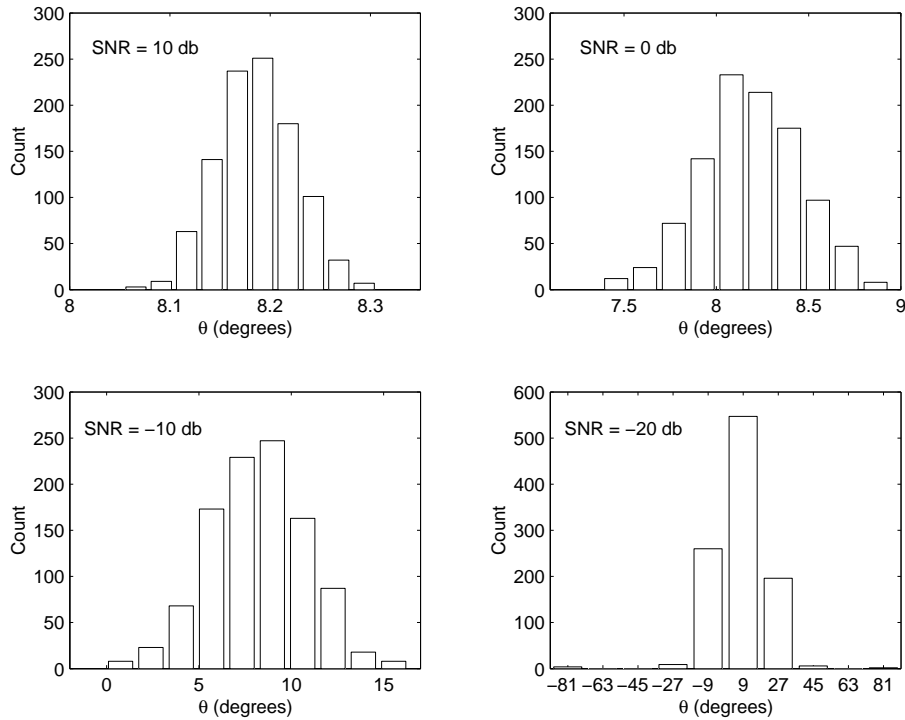
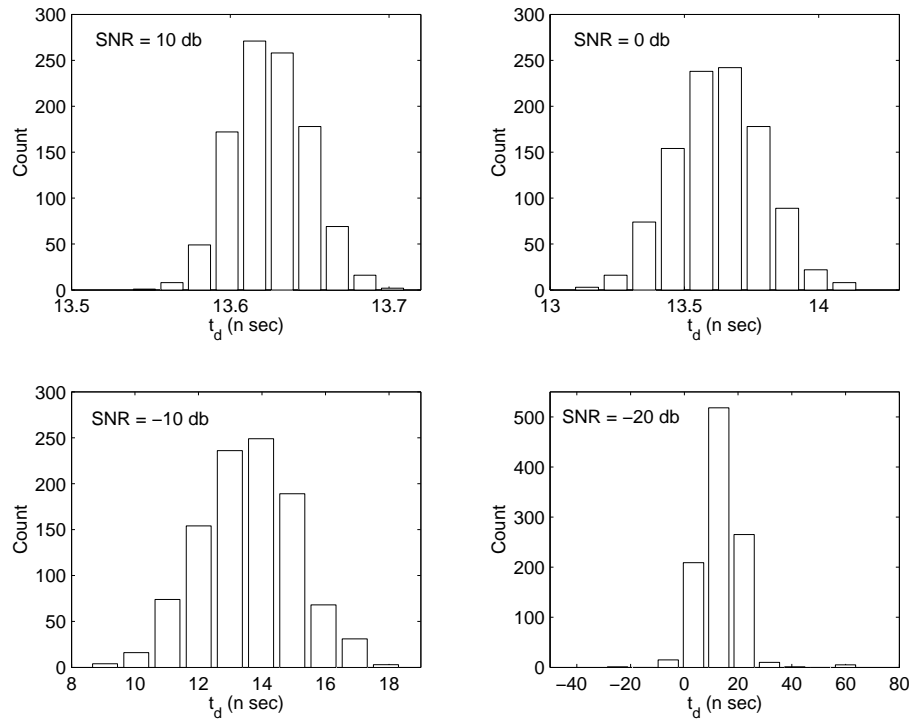
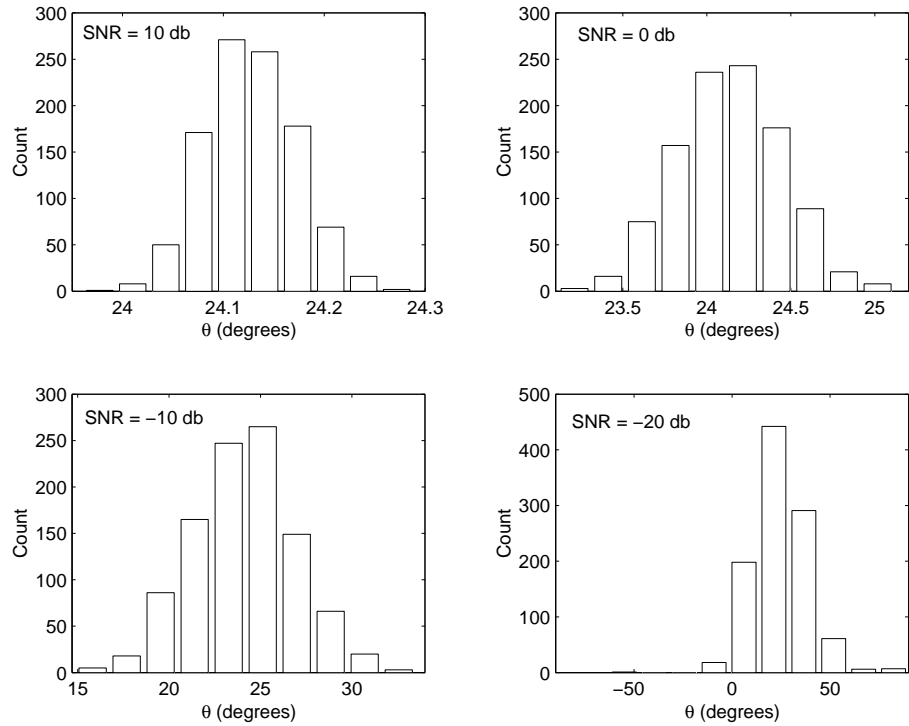


Figure 6: Angle estimate. $L = 10$ m, $\theta = 10^\circ$, CW

**Figure 7:** Time-delay estimate. $L = 10$ m, $t_d = 16.7$ n sec, CW**Figure 8:** Angle estimate. $L = 10$ m, $\theta = 30^\circ$, CW

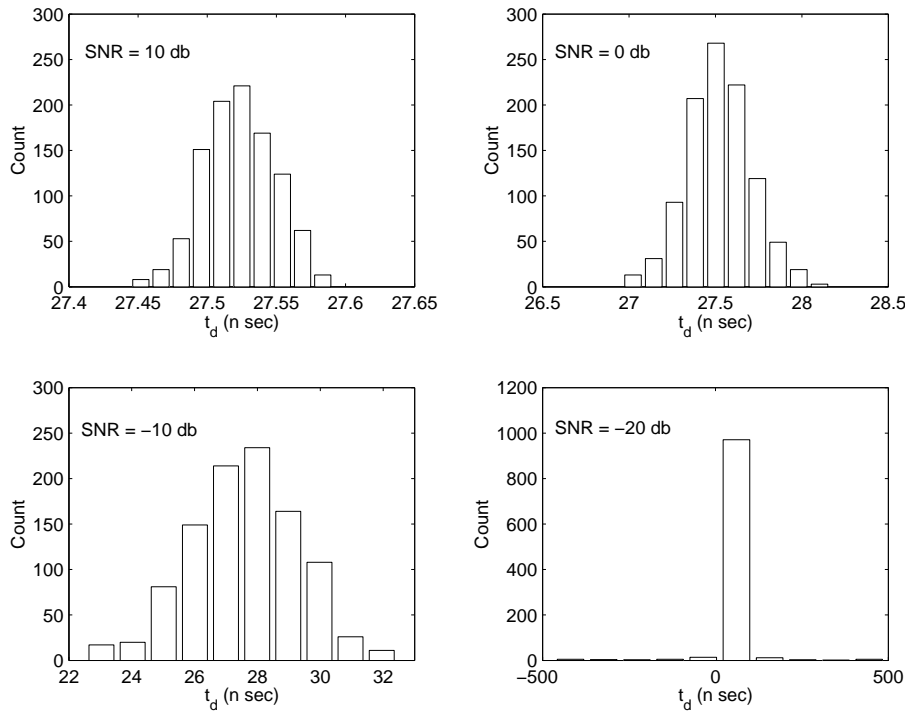


Figure 9: Time-delay estimate. $L = 10$ m, $t_d = 32.8$ n sec, CW

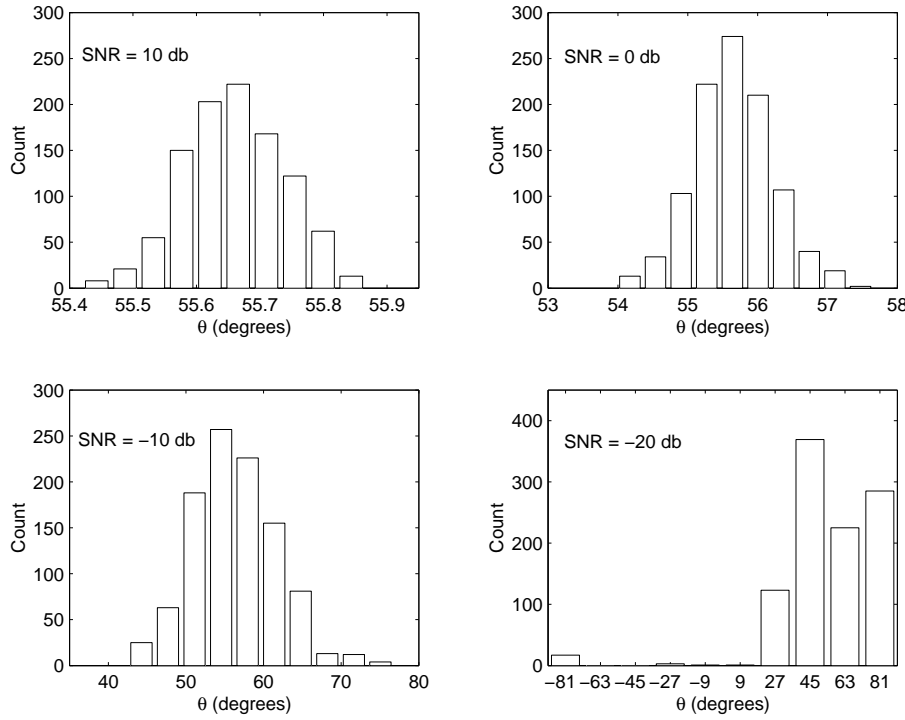


Figure 10: Angle estimate. $L = 10$ m, $\theta = 80^\circ$, CW

We see bias in Figures 5 to 10 for antenna separation of 10 m. We also note the large peaks at SNR below -10 dB. Although we may be tempted to use these values, we must take into account the large variance.

Again we note that these figures were generated from a simulation of 1024 iterations with 2^{18} data points. As such these estimates will be more accurate, and the variances smaller than we would expect from real data.

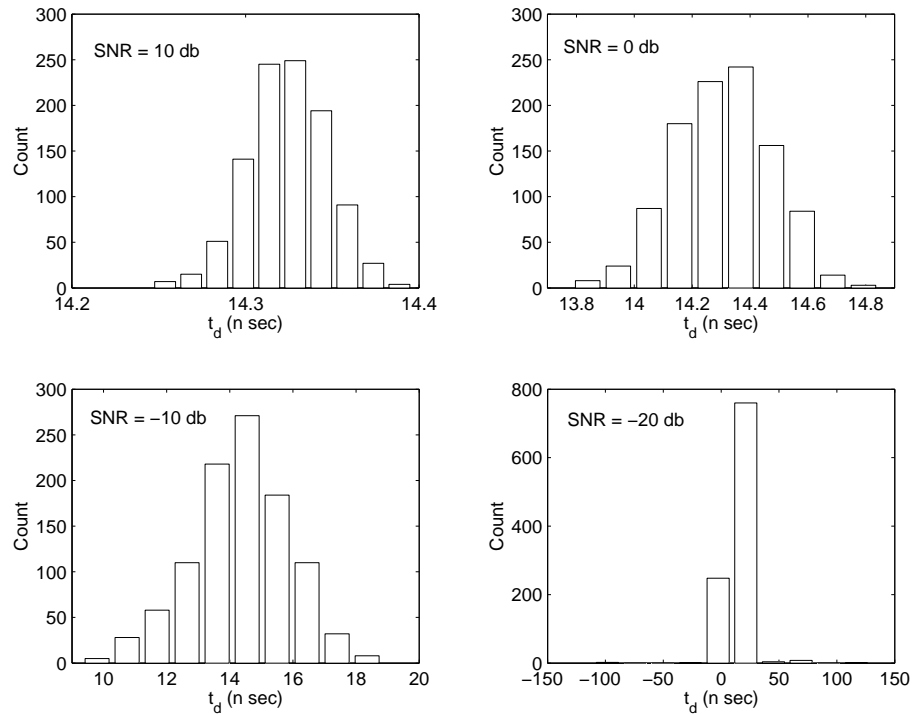


Figure 11: Time-delay estimate. $L = 30$ m, $t_d = 17.4$ n sec, CW

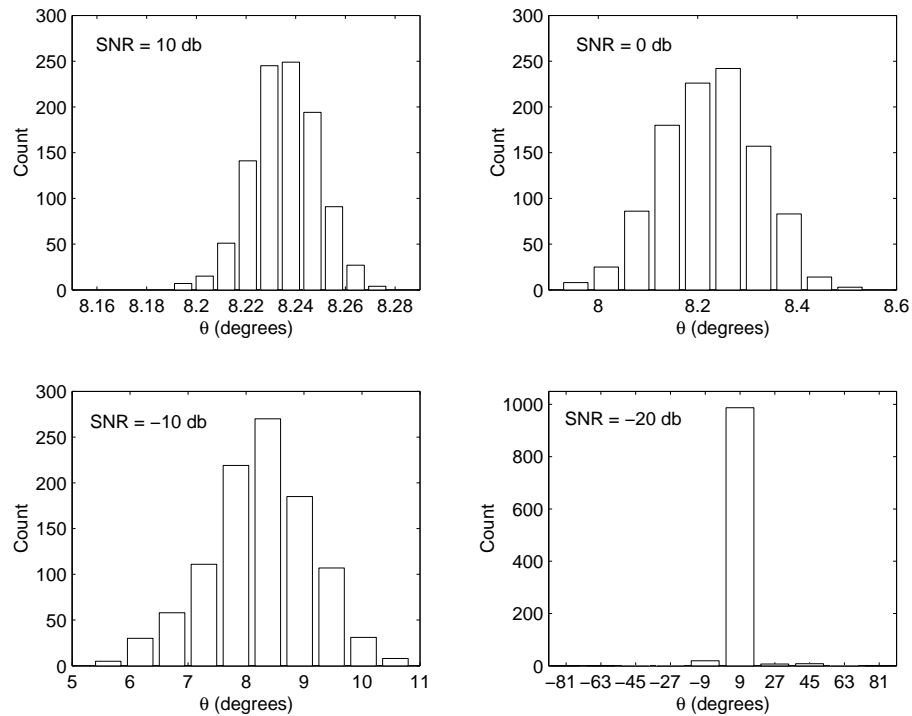


Figure 12: Angle estimate. $L = 30$ m, $\theta = 10^\circ$, CW

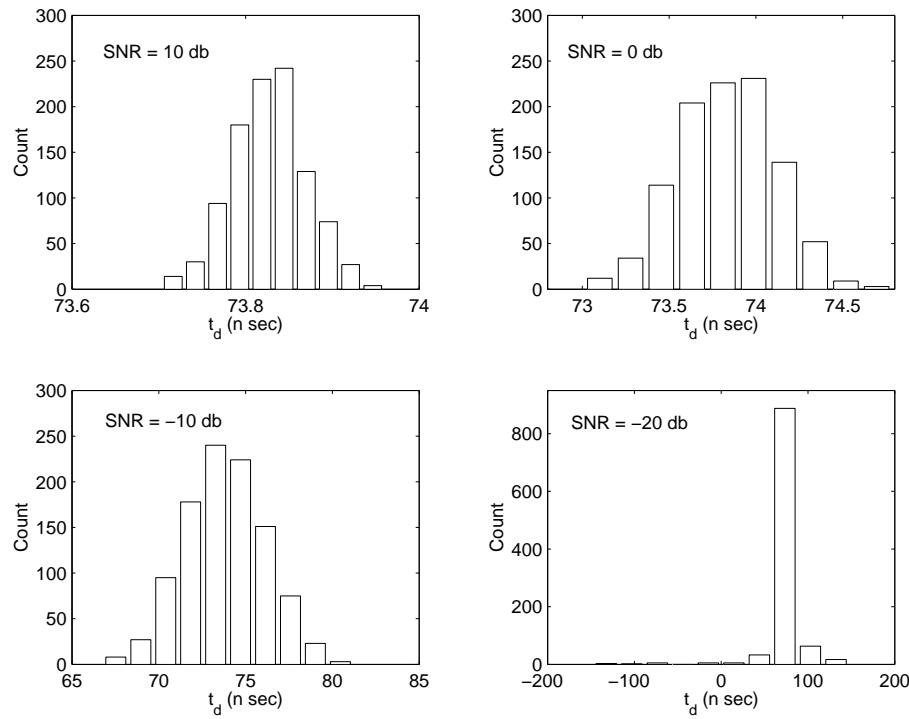


Figure 13: Time-delay estimate. $L = 30$ m, $t_d = 70.7$ n sec, CW

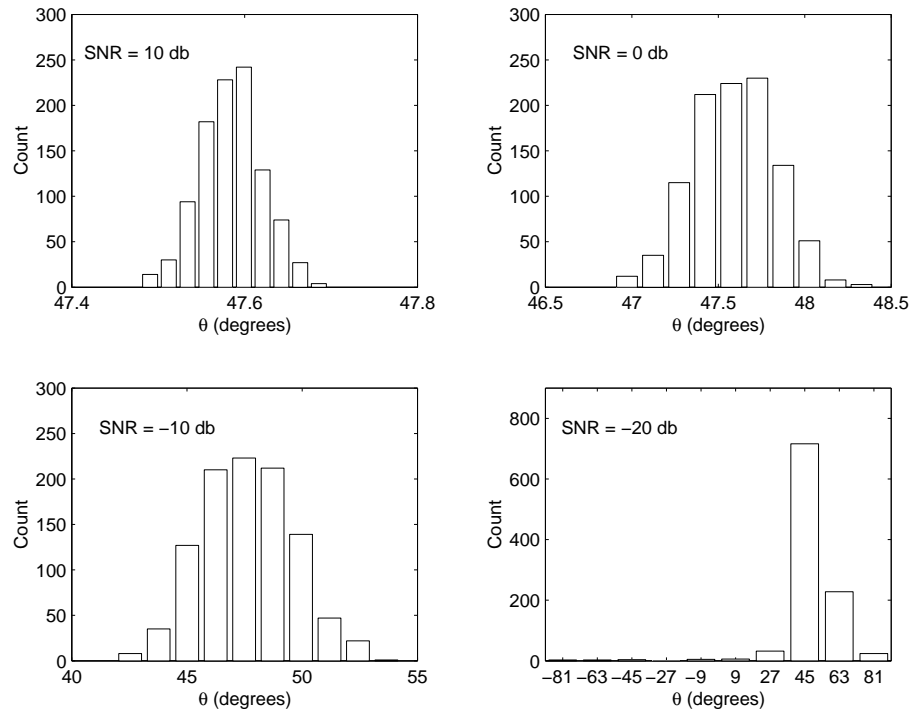


Figure 14: Angle estimate. $L = 30$ m, $\theta = 45^\circ$, CW

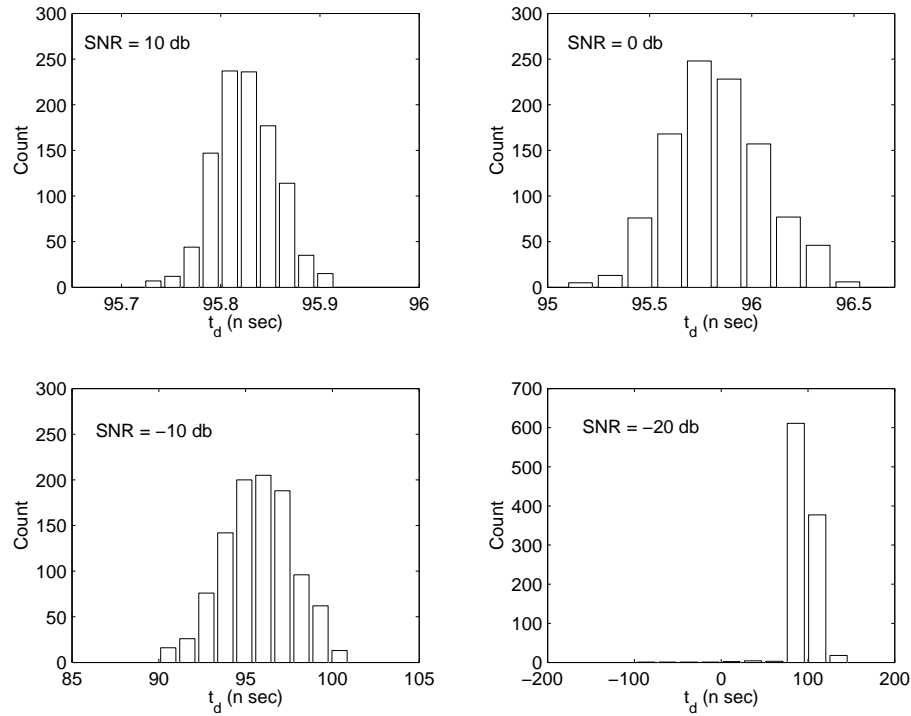


Figure 15: Time-delay estimate. $L = 30$ m, $t_d = 94$ n sec, CW

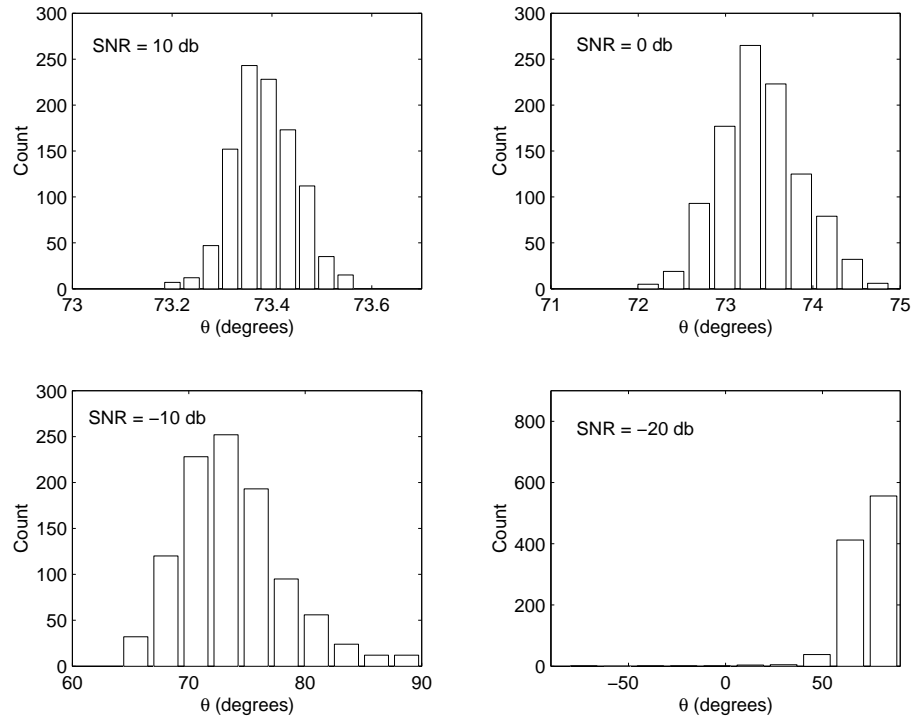


Figure 16: Angle estimate. $L = 30$ m, $\theta = 70^\circ$, CW

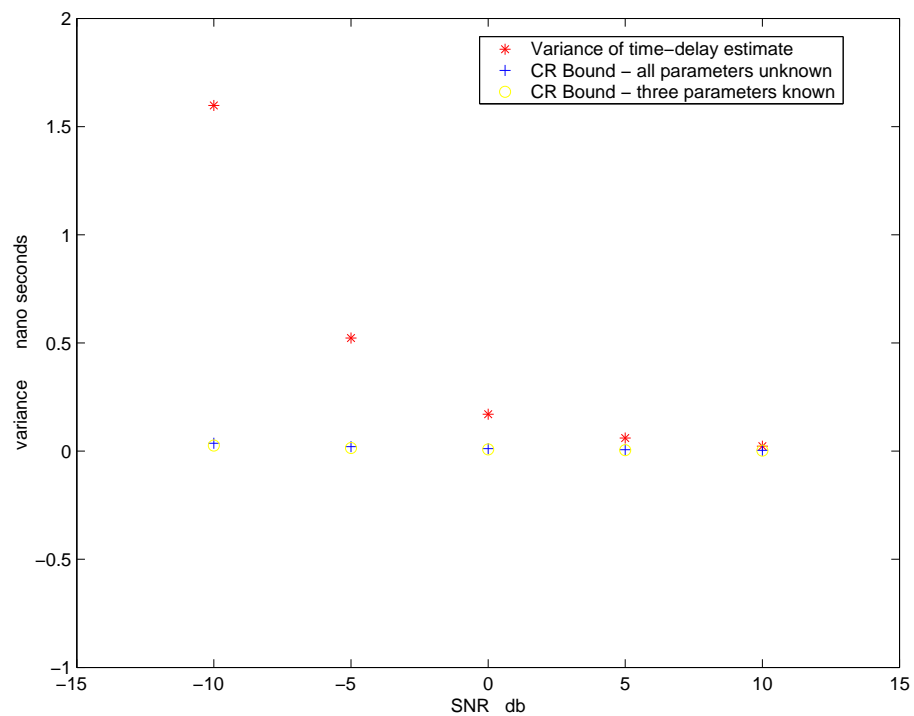


Figure 17: Variance versus SNR. $L = 10$ m, $\theta = 30^\circ$

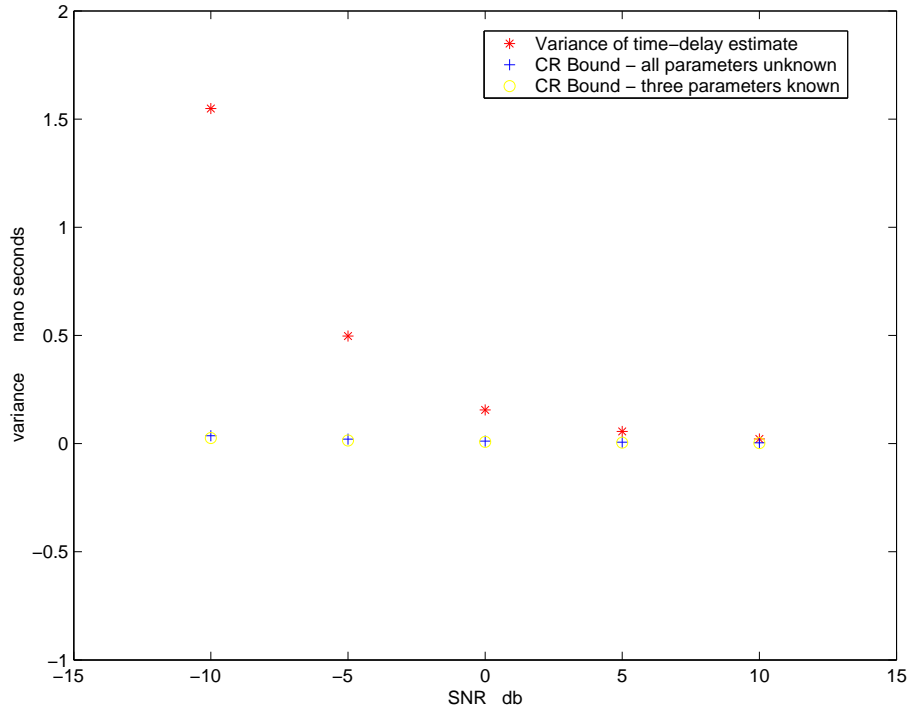


Figure 18: Variance versus SNR. $L = 10$ m, $\theta = 10^\circ$, CW

The above simulations suggest a bias in the estimate of time–delay, perhaps as a result of the frequency wrap around. For a receiver separation of 10 m, we see the difference between the actual time–delay and the estimated time–delay increasing as the angle of arrival increases. For an angle of arrival of 80° , and an SNR of 10 dB, we see the estimated time–delay differs from the actual time–delay by approximately 5 ns, or 25° . The actual time–delay in this case being 32.8 ns.

For a receiver separation of 30 m, the error is small and appears constant. This suggests small antenna separations may not be appropriate for CW signals.

2.3.2.2 Single Pulse

In Figures 21 to 32 we plot histograms of the estimate of the time–delay. The simulation used to estimate the time–delay ran over 1024 iterations, with 2^{18} data points. Sample rate is 5 ns. As with the CW case, we also give angle estimates. Angle estimates are obtained from the time–delay estimate after each iteration, by inverting Equation (50), and replacing t_d with \hat{t}_d .

In Figures 21 to 26, we fix the antenna separation at $L = 10$ m, and vary θ and SNR. In Figures 27 to 32, we fix the antenna separation at $L = 30$ m, and vary θ and SNR.

The estimate of the time–delay was taken to be the value with the maximum count number in the histogram. This value was then used in the estimate of angle.

Figure 19 was obtained using the Matlab specgram function [15]. There is no wrap–around.

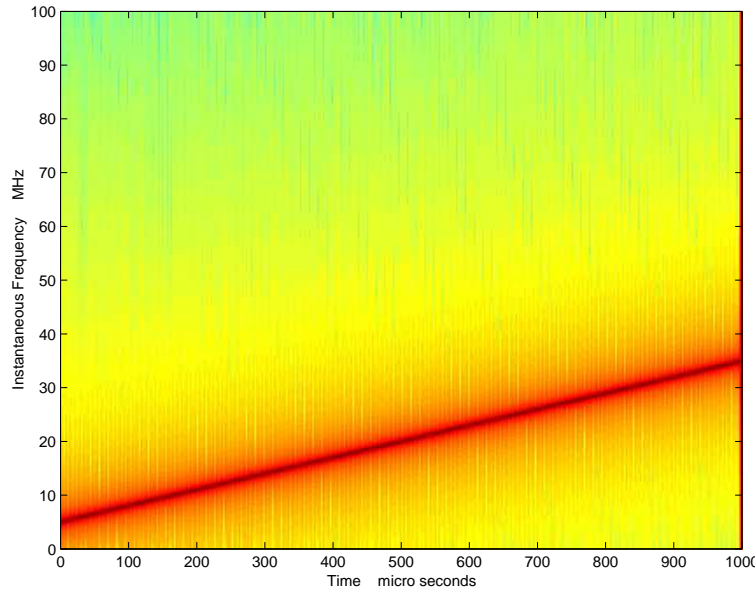


Figure 19: Instantaneous frequency of chirp waveform over sample time – single pulse

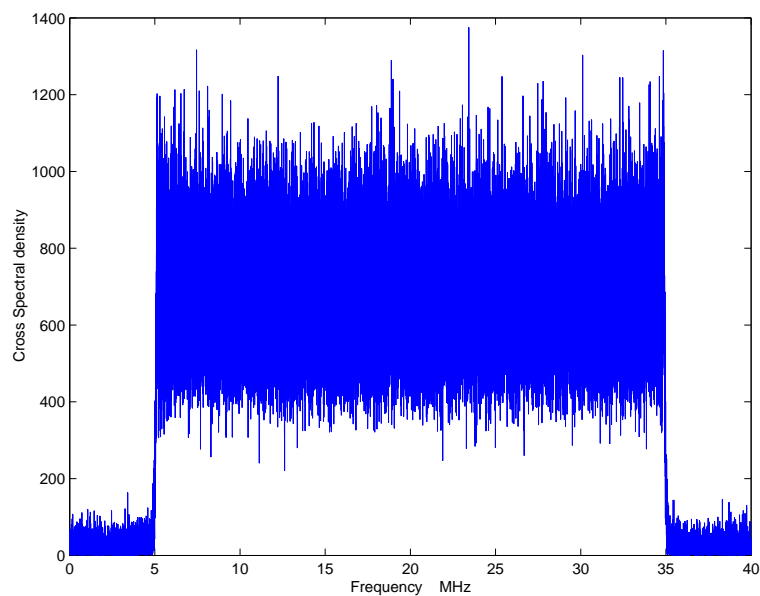


Figure 20: Cross Spectral Density – single pulse

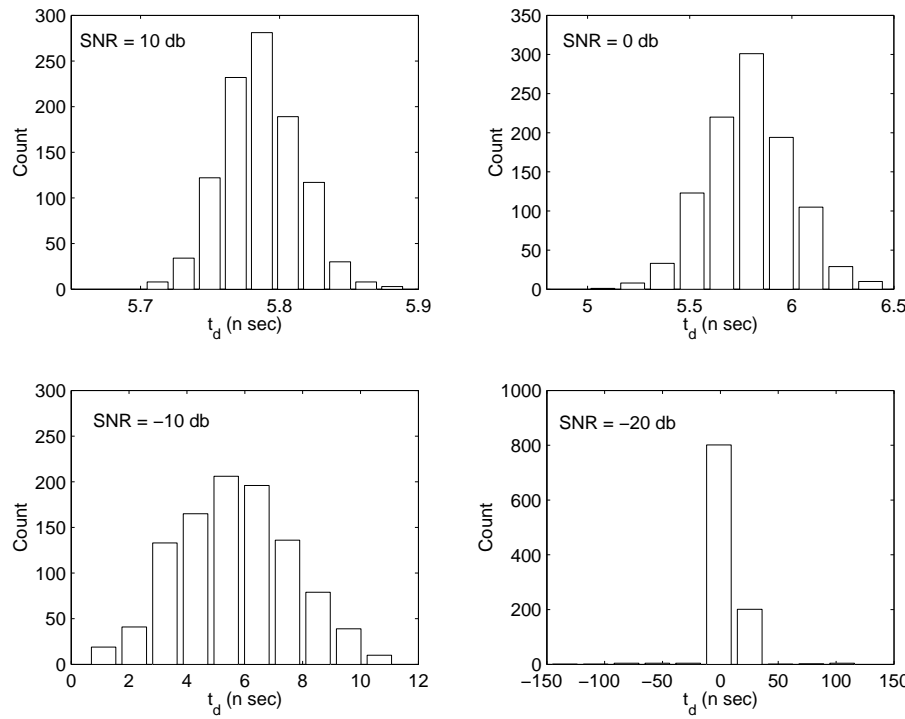


Figure 21: Time-delay estimate, $L = 10$ m, $t_d = 5.8$ ns, single pulse

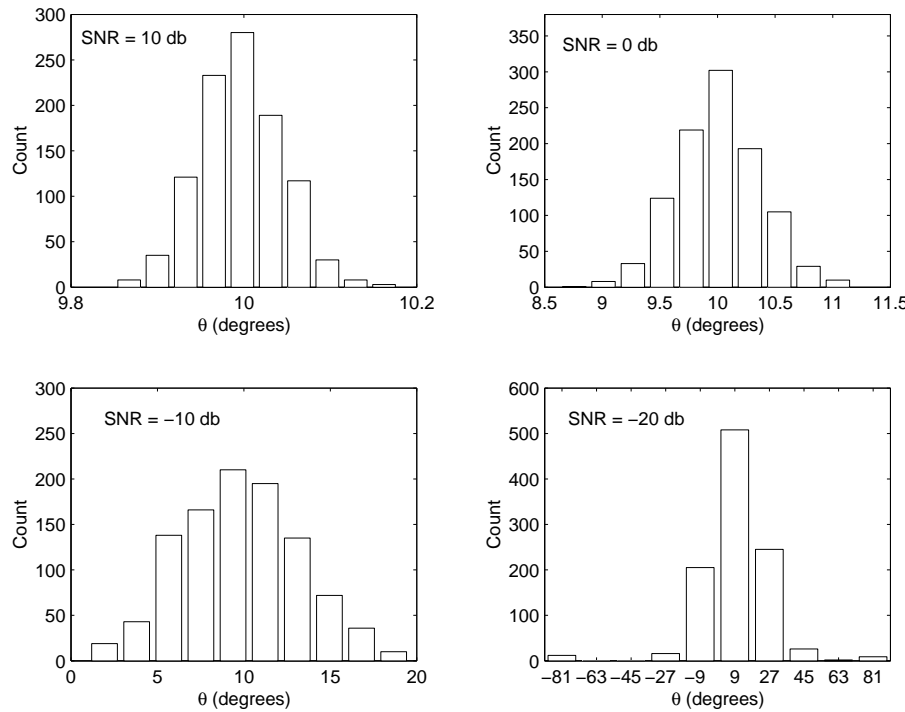


Figure 22: Angle estimate, $L = 10$ m, $\theta = 10^\circ$, single pulse

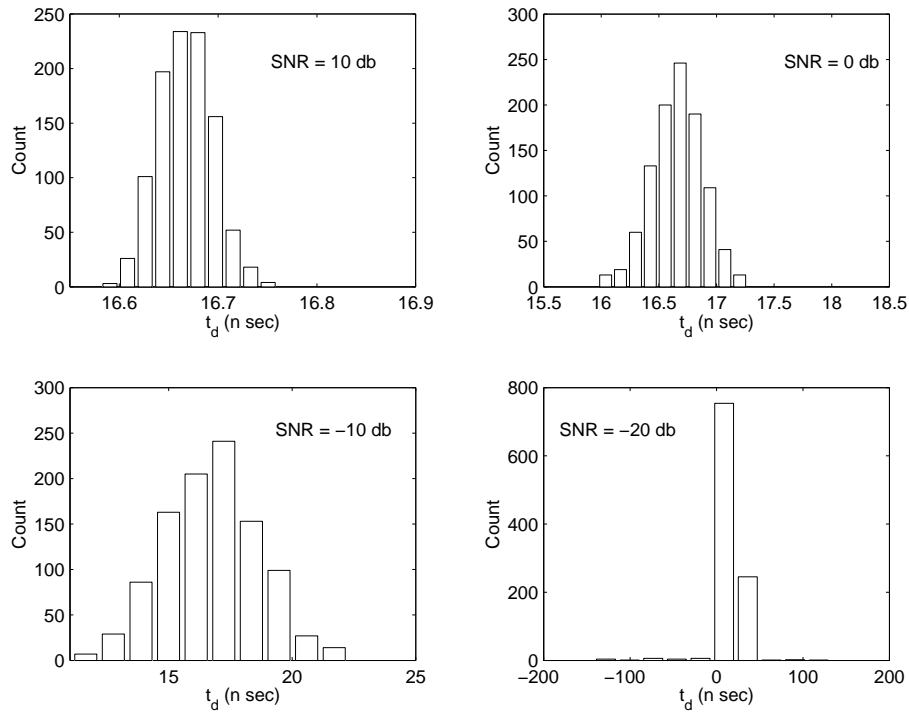


Figure 23: Time-delay estimate, $L = 10$ m, $t_d = 16.7$ ns, single pulse

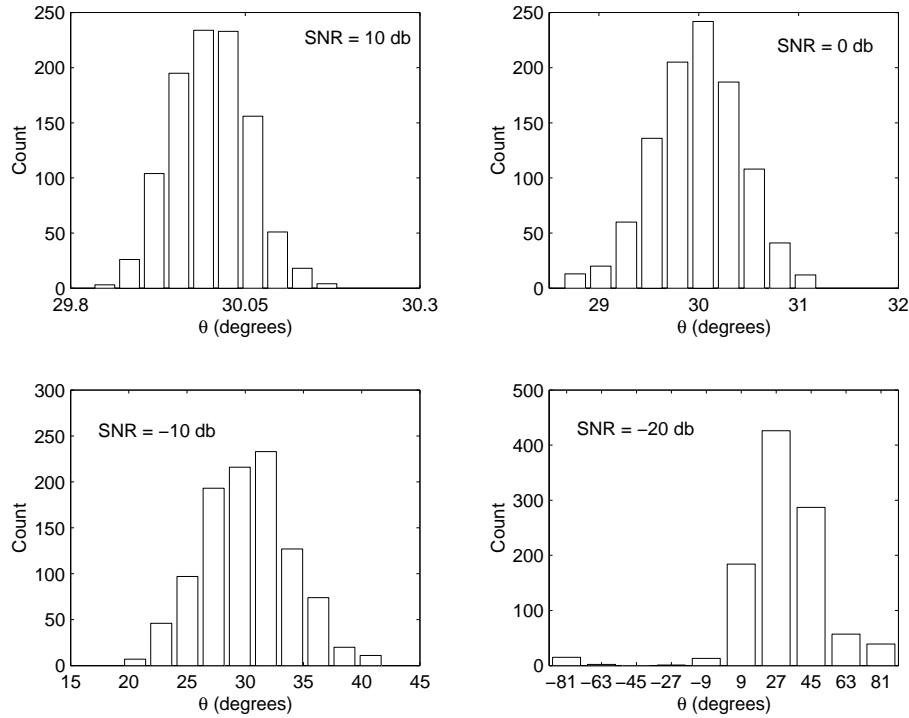


Figure 24: Angle estimate, $L = 10$ m, $\theta = 30^\circ$, single pulse

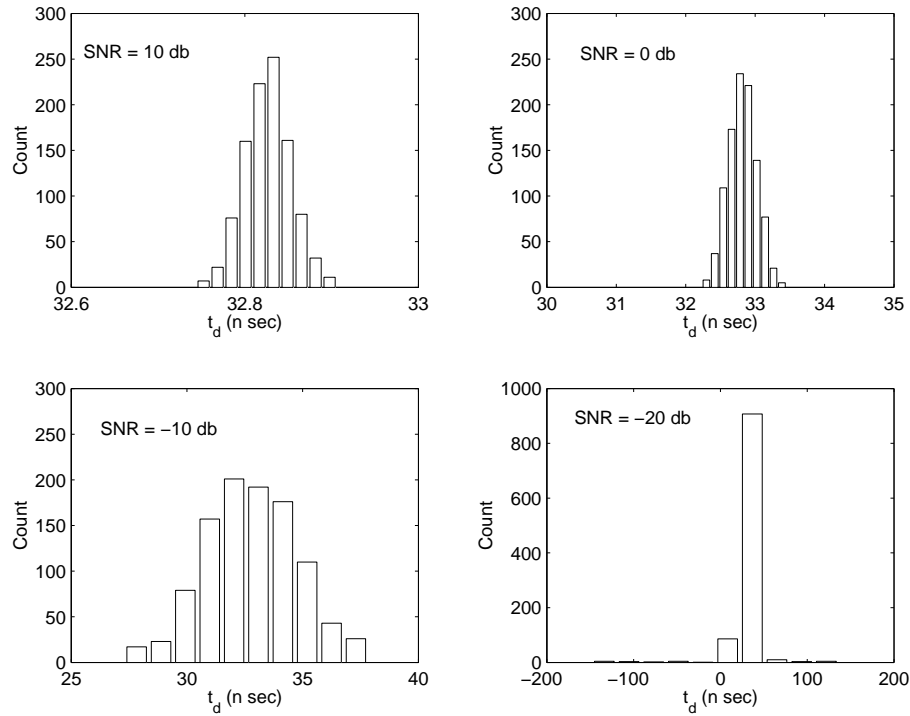


Figure 25: Time-delay estimate, $L = 10$ m, $t_d = 32.8$ ns, single pulse

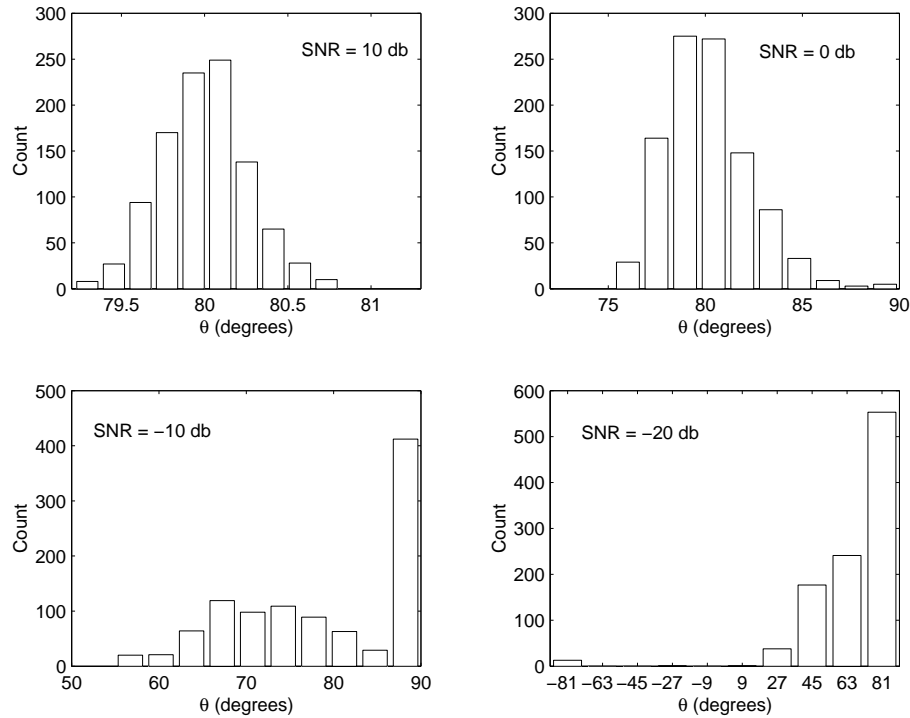


Figure 26: Angle estimate, $L = 10$ m, $\theta = 80^\circ$, single pulse

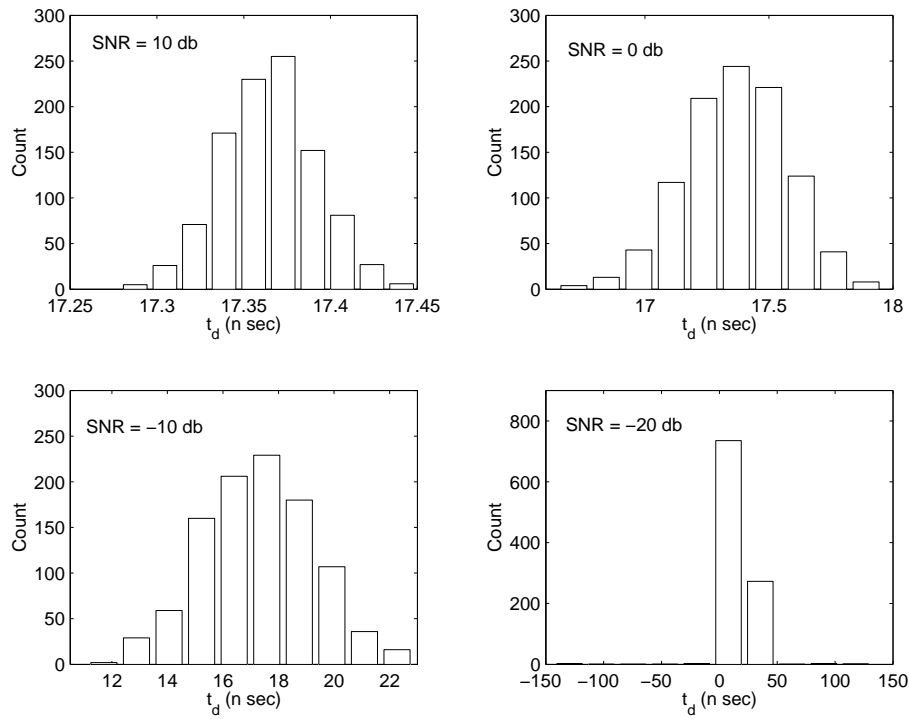


Figure 27: Time-delay estimate, $L = 30$ m, $t_d = 17.4$ ns, single pulse

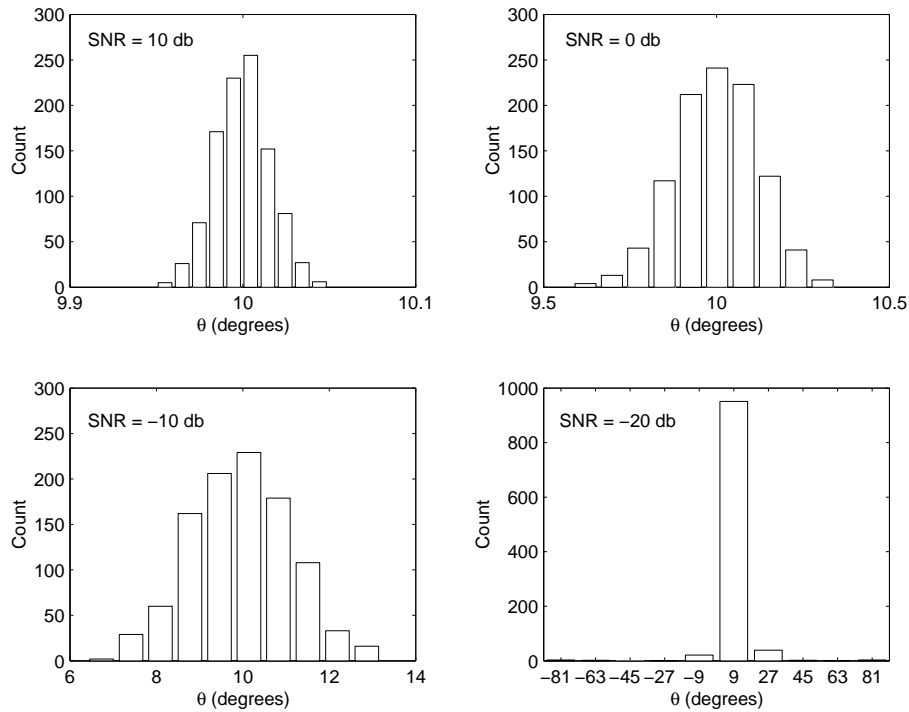


Figure 28: Angle estimate, $L = 30$ m, $\theta = 10^\circ$, single pulse

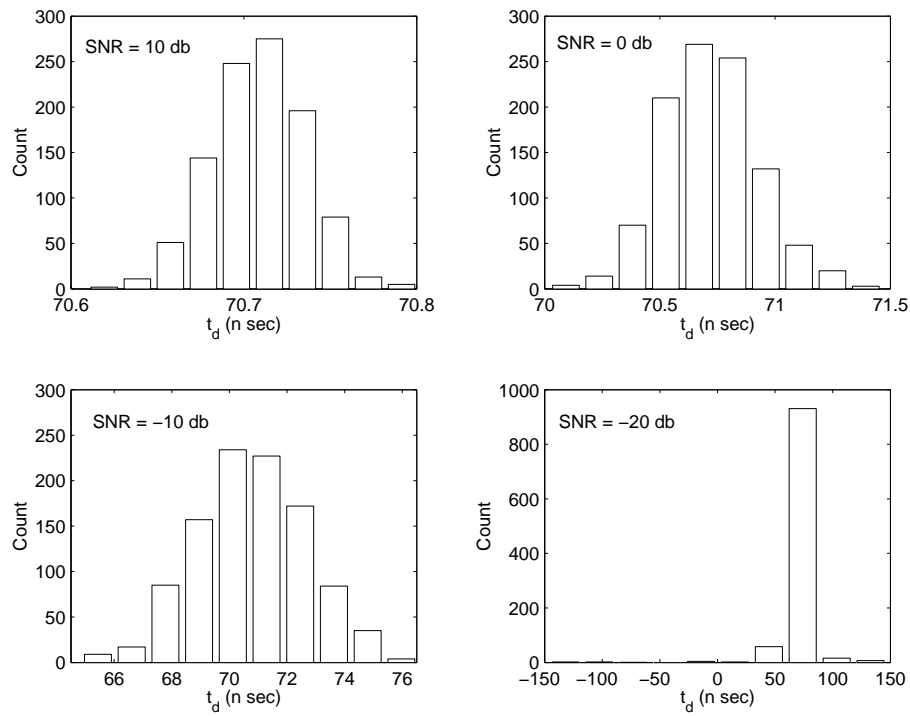


Figure 29: Time-delay estimate, $L = 30$ m, $t_d = 70.7$ ns, single pulse

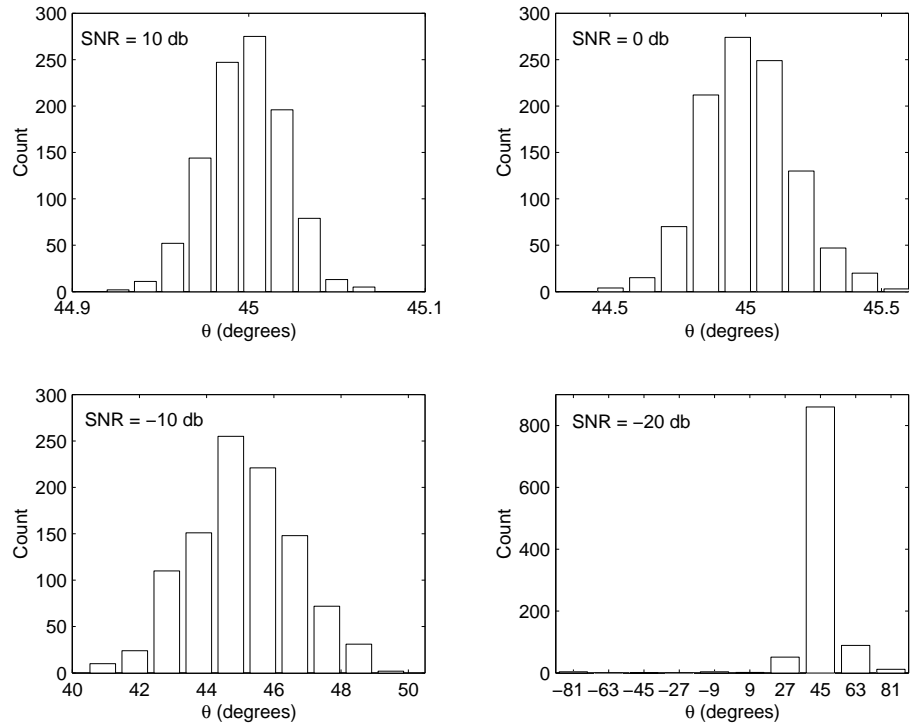


Figure 30: Angle estimate, $L = 30$ m, $\theta = 45^\circ$, single pulse

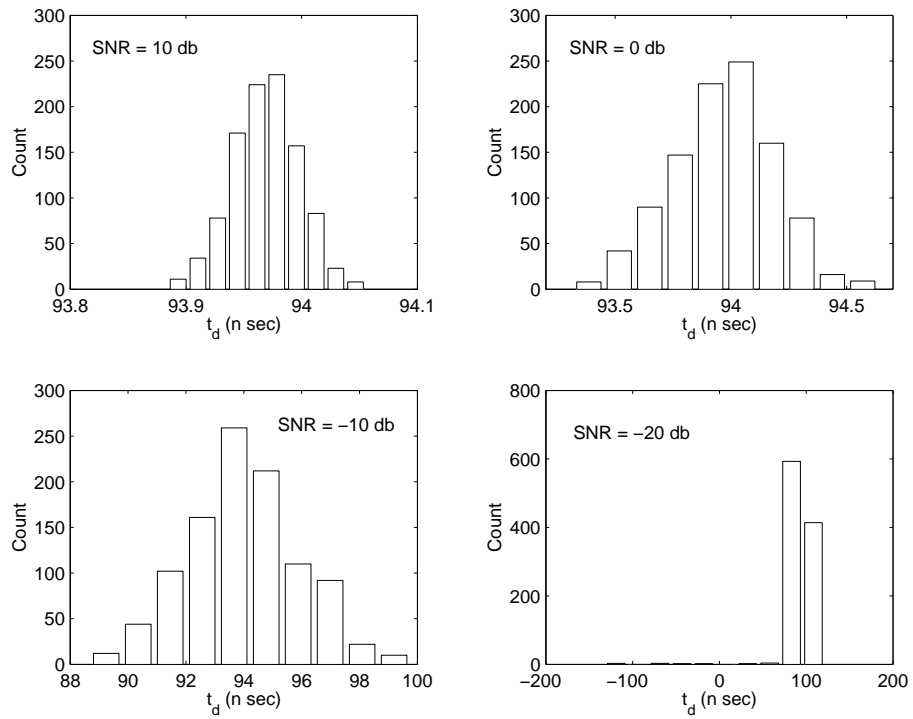


Figure 31: Time-delay estimate, $L = 30$ m, $t_d = 94$ ns, single pulse

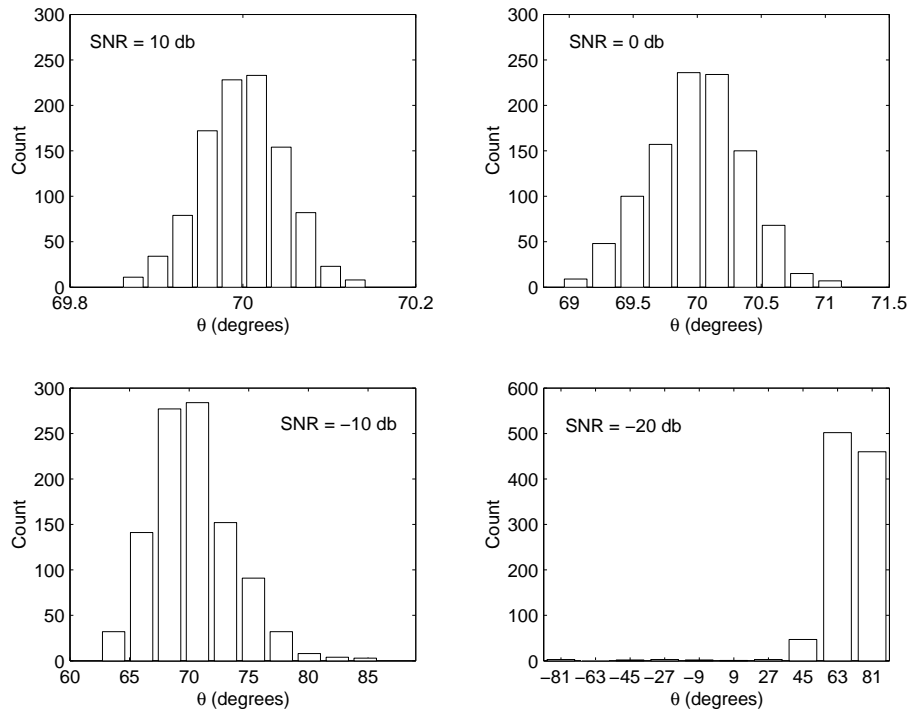


Figure 32: Angle estimate, $L = 30$ m, $\theta = 70^\circ$, single pulse

In contrast to the CW case, the single pulse simulations give estimates which are very close to the actual time-delay and angle of arrival values down to 0 dB. However the spread of values increases significantly as SNR decreases. We also assume that the correct signal has been detected at such a low SNR.

Again we note these estimates are expected to be more accurate, and the variances smaller than we would expect from real data.

3 EWRD Durex Trial Data

We now apply the techniques described earlier to data obtained from the EWRD Durex trial of 17 July, 2002 [1].

In Figure 33, we see the true time-delay as a function of angle. This figure shows that for large angle, small changes in time-delay represent large changes in angle. For this reason, good estimates will be found where the curve is not near the regions of maximum curvature – that is, for $-60^\circ < \theta < 60^\circ$.

The samples were of pseudo-random noise with 20 MHz bandwidth.

The receiver was dual channel, with 8 bit ADC, sampling at 200 MSps at 50 MHz IF. The two receivers were 29.5 m apart, with the straight line between antennas being 0° magnetic North.

The two receivers were not calibrated.

The transmitter was moved parallel to the receivers, with angle being measured using a compass. The last series of data were taken due south of the receivers.

The geometry of this setup is shown in Figure 34.

We compare the geometry of the Durex trial with that given by Figure 2, and observe that a mapping between the two conventions is needed. We see that the Durex trial definition of 90° , is the theoretical 0° . Similarly, 135° becomes -45° , 150° becomes -60° , and 22° becomes 68° .

We note that negative angles refer to receiver 1 lagging receiver 2.

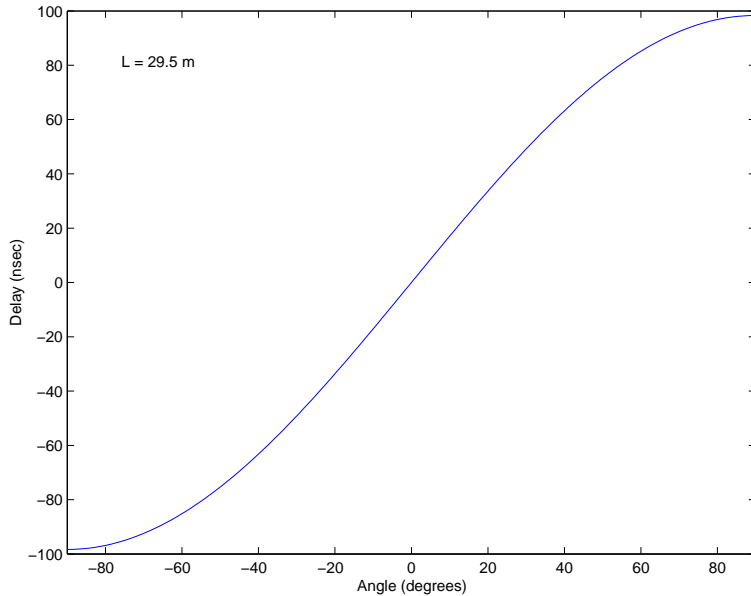


Figure 33: Time-delay as a function of angle

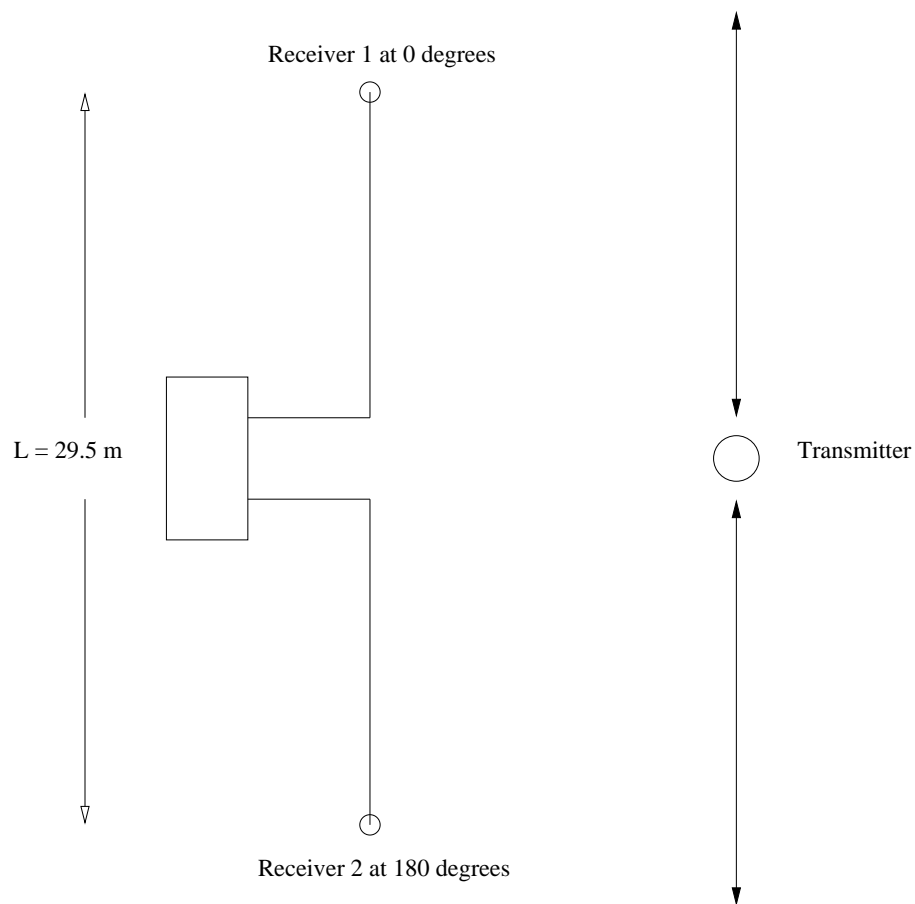


Figure 34: Receiver – Transmitter geometry, Durex trial

In Table 3.1, we present trial estimates of the angle. The angle given in column 4 is that found by a compass reading. Table 3.2, gives estimates of the time-delay. The time-delay given is the expected delay given the angle and receiver separation of 29.5 m.

Figure 35 shows time-delay as a function of angle. We have also plotted estimates of the time-delay, given in Tables 3.1 and 3.2.

Unfortunately, due to the nature of the data collection, we are unable to comment on the accuracy of the time-delay estimation method using the Durex trial data.

Table 3.1: Angle estimates from Durex trial data

File name	Tx Power (dBm)	Rx attenuation (dB)	Angle ($^{\circ}$)	Estimated Angle ($^{\circ}$) (averaged)
ADC001 – ADC009	39	25	0	-4.7
ADC010 – ADC019	39	25	-45	-35.2
ADC020 – ADC029	0	0	-45	-31.2
ADC030 – ADC039	0	0	-60	-41.8
ADC040 – ADC049	39	25	-60	-44.8
ADC080 – ADC089	39	25	0	2.2
ADC090 – ADC099	39	25	45	48.8
ADC100 – ADC109	39	25	68	77.3
ADC110 – ADC119	39	25	-90	-62.4

Table 3.2: Time-delay estimates from Durex trial data

File name	Tx Power (dBm)	Rx attenuation (dB)	Delay (ns)	Estimated Delay (ns) (averaged)
ADC001 – ADC009	39	25	0	-8.1
ADC010 – ADC019	39	25	-69.5	-56.7
ADC020 – ADC029	0	0	-69.5	-50.9
ADC030 – ADC039	0	0	-85.2	-65.5
ADC040 – ADC049	39	25	-85.2	-69.3
ADC080 – ADC089	39	25	0	3.8
ADC090 – ADC099	39	25	69.5	74
ADC100 – ADC109	39	25	91.2	95.9
ADC110 – ADC119	39	25	-98.3	-87.1

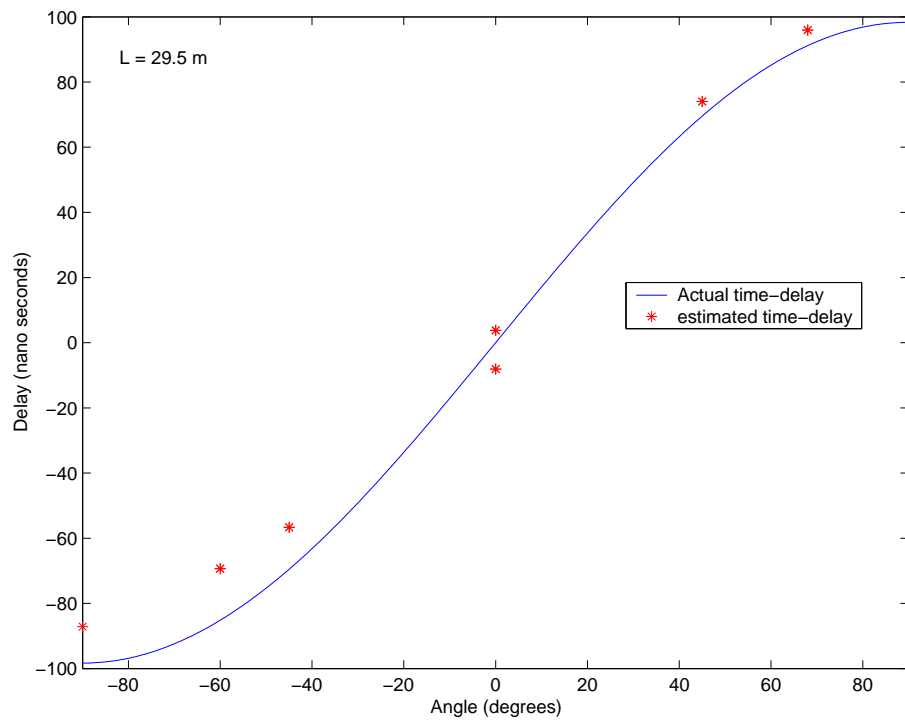


Figure 35: Durex trial, time-delay versus angle.

4 Time-Domain Filtered Cross Spectral Density

In the previous chapter, the algorithm for estimating time-delay was : start in the time domain with data from two spatially separated receivers. We move into the frequency domain by performing a Fourier transform on each data set. We suppress negative frequencies by generating an analytic signal via a Hilbert transform, and we multiply their Fourier transforms to produce the cross spectral density.

We then apply an inverse Fourier transform to this density to move back into the time domain, to give the cross correlation function. We time filter this function, to remove unnecessary data – away from the peak – and perform a quadratic interpolation on the filtered function to give us the time-delay estimate.

In [16], the cross correlation is performed in the time domain, and the cross spectral density is obtained via Fourier transform. The time-delay is estimated in the frequency domain from the phase slope of the cross spectral density.

Then a spread-spectrum signal arriving at two spatially separated receivers is cross correlated. The cross-correlation output will be the sum of 1) a time-delayed auto-correlation of the signal, 2) the cross correlation of the signal with noise, and 3) the cross-correlation of the noise.

The noise cross-correlation component will be spread uniformly over the entire cross-correlation function. The auto-correlation component will peak near the center of this function. The shift from the center represents the time-delay. However, noise will ensure the peak does not occur at the actual time-delay, so it is not possible to just “read off” the value from the plot, with reasonable accuracy.

Knowing that the auto-correlation component will be concentrated over a region tens of nanoseconds wide, we can apply a low pass time-domain filter. An FFT applied to this filtered function leads to the time-domain filtered cross spectral density. It also leads to phase wrapping. The phase slope of this density, across the signal bandwidth, is the estimate of the angle of arrival [16].

If the signal is shifted by an amount t_d , then the rate of change of phase with frequency is proportional to t_d . Once the time-domain filtered cross spectral density has been obtained, the phase slope can be estimated using linear regression. From this, we estimate time-delay.

We mentioned that the application of the FFT leads to phase wrapping. Therefore, we need to unwrap the phase before we make a straight-line fit. This requires any phase errors at each sample to be small. It has been shown that the phase errors due to noise are small if $\text{SNR} > 13 \text{ dB}$ [16, 17].

The angle of arrival estimation error is found to be similar in form to Equation (A14). It was found that high accuracy can be obtained (fractions of a degree), with large errors found for $|\theta| > 60^\circ$. The estimate is also shown to be independent of the receiver noise bandwidth and the “size” of the time-domain filtering, providing it is large enough to enable detection.

5 Discussion

The preceding was a technical report on the usefulness of exploiting the waveform design of highly correlated LPI signals, in order to estimate time-delay, and as a result, angle of arrival. The model consisted of two stationary receivers spaced several metres apart. The signal source is also assumed to be stationary.

For the simulations, we considered a chirped signal. The time taken from the lowest to highest frequency value was 1 ms. The signal was sampled evenly, the sample rate being 5 ns, at various SNRs, and the time-delay estimated, as described in the report. Quadratic interpolation was used to obtain sub sample rate estimates. For the purpose of simulation, we used 2^{18} data points, and 1024 iterations. As a result, we can expect our estimates to be more accurate, and our variances smaller than would be expected from real data.

We considered the case of a continuous wave (CW) signal, and a single pulse. The CW case allowed us to observe the effects of frequency wrap around on the estimates. For the CW signal, the sample time is just over 1 ms, allowing for frequency wrap around. For the pulsed signal, sample time is the pulse duration, which is 1 ms.

We started the simulation with a CW signal, a receiver separation of 10 m, and a true time-delay of 5.8 ns, representing a true angle of arrival of 10° . As we found in Section 2.3.2, our time-delay estimates were off by approximately 1 ns, or approximately 2° . That is, at an SNR of 10 dB, and a true time-delay of 5.8 ns (10°), we estimated the time-delay to be 4.8 ns, with a variance of 0.02 ns. This time-delay estimate represents an angle of arrival estimate of 8.2° .

Even at -10 dB SNR, we estimated the time-delay to be 4.9 ns. However, the variance was 1.5 ns, with the spread of estimates far greater than those found at 10 dB.

We then increased the true time-delay (or angle of arrival) for the same antenna separation of 10 m. We found the estimates differed from the true values by an increasing amount. That is, at 10 dB, for a true time-delay of 16.7 ns (30°), we estimated 13.7 ns (24.1°). For a true time-delay of 32.8 ns (80°), we estimated 27.5 ns (55.7°).

We then increased antenna separation to 30 m, and repeated the simulations but with different time-delays. In this case, at 10 dB, we found the difference between the true time-delay and the estimated time-delay to be approximately 2 to 3 ns.

At 10 dB, for a true time-delay of 17.4 ns (10°), we estimated 14.3 ns (8.2°). For a true time-delay of 70.7 ns (45°), we estimated 73.8 ns (47.6°). For a true time-delay of 94 ns (70°), we estimated 95.8 ns (73.4°).

As SNR decreased we found the estimates to be constant, although the spread of estimates increased.

The above suggests, for CW signals, there may be an optimum antenna separation for which estimates are reasonably accurate, and errors are small for all angles of arrival.

Repeating the above for a pulsed signal produced results more accurate than the above.

For a receiver separation of 10 m, and a true angle of arrival of 30° , representing a true time-delay of 16.7 ns, we estimated the time-delay to be 16.7 ns, with a variance of 0.03 ns. This time-delay estimate represents an angle of arrival estimate of 30° .

For a receiver separation of 10 m, and a true angle of arrival of 10° , representing a true time-delay of 5.8 ns, we estimated the time-delay to be 5.8 ns, with a variance of 0.03 ns. This time-delay estimate represents an angle of arrival estimate of 10° .

This analysis suggests that, even with SNR at -10 dB, this method gives a reasonable measure of the time-delay, or angle of arrival. However, the spread of estimates may negate the usefulness of such estimates, as well as the need to actually observe a signal at such a low SNR.

We have also tested this approach against pseudo-random noise generated during the EWRD Durex trial. Due to the data obtained, we were unable to comment on the accuracy of our estimation method.

Possible future research :

When estimating the time-delay, we made use of a quadratic interpolation, in order to achieve sub sample rate accuracy. This, however, leads to a biased estimate [11].

The pulsed case seems to suggest this bias will be small. This may not be so for the CW case, although the frequency wrap around effect may well dominate any bias. This could be investigated further.

It is also possible that this bias can be reduced by ‘windowing’.

The approach described in this report should be tested against Pilot-like signals [22], with accurate ground truth. This will also suggest the amount of data needed for accurate estimation in “real world” situations.

Our approach to calculating the Cramer–Rao bounds was a “brute force” approach, with a number of assumptions.

Is there a model in which the signal functions in the two receivers are orthogonal? This would remove the cross terms from the log likelihood function.

The obvious case would be to have the signal in the second receiver 90° out of phase with the signal in the first receiver. This, however, is highly unlikely to occur.

Re-writing the problem in terms of analytic functions may be useful [2].

One obvious generalisation to the theory given in this report would be to include a second signal source, and consider the detection and estimation problem [23, 24].

Another would be to consider moving sources and/or receivers.

6 Acknowledgments

The author would like to acknowledge the assistance of S.Howard, who proposed this work (under Task ADA 95/356), D.Driscoll, G.Noone, S.Elton and T.Douglas. He would like to thank D.Driscoll for the Matlab code used in Section 2.3.2, and thank J.Quin for the data used in Chapter 3, and for the Matlab code used to read the data.

References

1. Quin J., "Durex Trial Report." Unpublished (2002).
2. Rihaczek A., "Principles of High-Resolution Radar". Artech House (1996).
3. Van Trees H.L., "Detection, Estimation, and Modulation Theory. Part III". John Wiley and Sons(1971).
4. Woodward P.M., "Probability and Information Theory, with Applications to Radar". Artech House (1980).
5. Deley G.W. in "Radar Handbook". Ed. M.I. Skolnik. McGraw-Hill (1970).
6. Gabor D., "Theory of Communication". J. IEE, vol.93, pt.III, pp. 429 – 457 (1946).
7. Cook C.E. and Bernfeld M., "Radar Signals. An Introduction to Theory and Application". Artech House (1993).
8. Stein S., "Algorithms for Ambiguity Function Processing". IEEE Trans. Acoust., Speech, Signal Processing, vol. ASSP-29, no. 3, pp 588 – 599 (1981).
9. Hahn S.L., "Hilbert Transforms in Signal Processing". Artech House (1996).
10. Proakis J.G. and Manolakis D.G., "Digital Signal Processing : Principles, Algorithms, and Applications". Prentice Hall (1996).
11. Boucher R.E. and Hassab J.C., "Analysis of Discrete Implementation of Generalized Cross Correlator". IEEE Trans. Acoust., Speech, Signal Processing, vol. ASSP-29, no. 3, pp 609 – 611 (1981).
12. Moddemeijer R., "On the Determination of the Position of Extrema of Sampled Correlators". IEEE Trans. Signal Processing, vol 39, no. 1, pp 216 – 219 (1991).
13. Jacovitti G. and Scarano G., "Discrete Time Techniques for Time Delay Estimation". IEEE Trans. Sig. Proc., vol. 41, pp 525 – 533 (1993).
14. Rife D.C. and Boorstyn R.R., "Single-Tone Parameter Estimation from Discrete-Time Observations". IEEE Trans. Inform. Theory, vol. IT 20, pp 591–598 (1974).
15. "Matlab. The Language of Technical Computing." The MathWorks Inc. (2005).
16. Houghton A.W. and Reeve C.D., "Direction finding on spread-spectrum signals using the time-domain filtered cross spectral density". IEE Proc. Radar, Sonar Navig., Vol 144, No. 6, pp 315 – 320 (1997).
17. Houghton A.W. and Reeve C.D., "Detection of spread-spectrum signals using the time-domain filtered cross spectral density". IEE Proc. Radar, Sonar Navig., Vol 142, No. 6, pp 286 – 292 (1995).
18. MacDonald V.H. and Schultheiss P.M., "Optimum Passive Bearing Estimation in a Spatially Incoherent Noise Environment". J. Acoust. Soc. Amer., vol. 46, pp 37 – 43 (1969).

19. Knapp C.H. and Carter G.C., "The Generalised Correlation Method for Estimation of Time Delay". IEEE Trans. Acoust. Speech, Signal Processing, vol. ASSP-24, pp 320 – 327 (1976).
20. "Coherence Estimation". Ed. Carter G.C and Nuttall A.H. Naval Underwater Systems Center (1979).
21. "Coherence and Time Delay Estimation". Ed. Carter G.C. IEEE Press (1993).
22. Fuller K.L., "To see and not be seen". IEE Proc., vol. 137, pt. F, pp 1 – 9 (1990).
23. Rife D.C. and Boorstyn R.R., "Multiple Tone Parameter Estimation from Discrete-Time Observations". The Bell Systems Technical Journal, vol. 55, No. 9 pp 1389–1410 (1976).
24. Ng L.C. and Bar-Shalom Y., "Multisensor Multitarget Time Delay Vector Estimation". IEEE Trans. Acoust., Speech, Signal Processing, vol. ASSP-34, no. 4, pp 669 – 677 (1986).

Appendix A Optimum Passive Bearing Estimation

The paper of MacDonald and Schultheiss [18] considers the problem of ‘optimum passive bearing estimation by means of a passive sonar array’. They consider M hydrophones arranged in a linear array. The following uses $M = 2$.

Four assumptions are made

1. The signal and noise are stationary Gaussian processes.
2. The signal source is at such a distance from the receivers, that the received wavefront is planar over the dimensions of the receiving system.
3. Noise is statistically independent from each other and the signal.
4. The observation time T is much larger than the signal and noise correlation time and the travel time of the wavefront across the receiving system.

They start by finding the Cramer–Rao lower bound of the unbiased estimators rms error. They then compare this to the rms error from a split-beam tracker. The comparison suggests that the split-beam tracker is close to optimal.

A.1 Cramer–Rao Bound

Over the observation time T , we have (continuous time) data received at antenna A

$$x_A(t) = s_A(t) + n_A(t) \quad (\text{A1})$$

and at antenna B

$$x_B(t) = s_A(t - t_d) + n_B(t) \quad (\text{A2})$$

We see explicitly that the data received at antenna B is the time-delayed data received at antenna A. The aim is to estimate the time-delay t_d , denoted \hat{t}_d , and the variance of this estimate, denoted $\sigma_{\hat{t}_d}^2$, given the data.

The minimum variance of an unbiased estimate is the Cramer–Rao bound, and is

$$\sigma_{\hat{t}_d}^2 \geq \frac{-1}{E\left[\frac{\partial^2 L(x)}{\partial t_d^2}\right]} \quad (\text{A3})$$

where E denotes the expectation, and $L(x)$ is the likelihood function, or more commonly, the log likelihood function. The likelihood function may be found via the Fourier coefficients of the received data.

We are able to perform Fourier transforms on this data in order to create a new vector. Let

$$\begin{aligned} X_A(k) &= \int x_A(t) e^{-i2\pi k \frac{t}{T}} dt \\ X_B(k) &= \int x_B(t) e^{-i2\pi k \frac{t}{T}} dt \quad k = 1 \dots N \end{aligned} \quad (\text{A4})$$

Then a new $2N \times 1$ vector can be written

$$X = [X_A(1) X_A(2) \dots X_A(N) X_B(1) X_B(2) \dots X_B(N)]' \quad (\text{A5})$$

where the ' superscript refers to the transpose operation.

The complex probability density function (pdf) for X can be written

$$\begin{aligned} p(X) &= \frac{1}{\pi^N \pi_{j=1}^N \sigma_j^2} \frac{1}{\pi^N \pi_{j=1}^N \sigma_j^2} e^{-\sum_{j=1}^N \frac{1}{\sigma_j^2} (X_A^{*'}(j) X_A(j) + X_B^{*'}(j) X_B(j))} \\ &= \frac{1}{\pi^{2N} |\Sigma|} e^{-X^{*'} \Sigma^{-1} X} \end{aligned} \quad (\text{A6})$$

where the * refers to complex conjugation. Here $|\Sigma|$ is the determinant of the $2N \times 2N$ covariance matrix Σ (not $4N \times 4N$ as $X(k) = X^*(T - k)$, so not all the vectors are independent).

As [18] dealt with bearing estimation, we continue the analysis in terms of the angle of arrival θ .

The covariance matrix $\Sigma = E[X^* X']$, and the matrix elements are

$$E[X_p^*(\omega_l) X_q'(\omega_n)] = \int_{-T/2}^{T/2} \int_{-T/2}^{T/2} e^{i(\omega_l t - \omega_n u)} E[x_p(t) x_q(u)] dt du \quad (\text{A7})$$

where $x(t) = x(t, \theta)$ is a function of the angle to be estimated. That is, $x_p(t, \theta) = s_A(t - t_{d_p}) + n_p(t)$, $p = A, B$, with $t_{d_A} = 0$ and $t_{d_B} = (d/c) \sin \theta$. Here d is the antenna separation and c the speed of light.

At this point we substitute for $x(t)$ in the expectation, and write the derived auto-correlation functions for the signal and noise in terms of the corresponding spectral functions, remembering that the signal and noise are assumed to be stationary processes.

Working through the analysis, it is found that

$$\begin{aligned} E[X_p^*(\omega_l) X_q'(\omega_n)] &= T[S(\omega_n) + N(\omega_n) \delta_{pq}] e^{i\omega_n(d_q - d_p)} & l = n \\ &= 0 & l \neq n \end{aligned} \quad (\text{A8})$$

where $S(\omega)$ and $N(\omega)$ are the signal and noise spectral functions, respectively, and δ_{pq} is the Kronecker delta function.

The result of this is to separate out the frequency components in the quadratic $X^{*'} \Sigma^{-1} X$, and reduce the original matrix with $2N \times 2N$ elements to a matrix with $4N$ non-zero elements.

As a result of this reduction, we can reduce the complexity of the matrix multiplications by writing the quadratic $X^{*'} \Sigma^{-1} X$, as the sum of N matrix products of the form $A^* B A$, where A is $1 \times N$, and B is $N \times N$. Each matrix product involves a particular frequency.

As a simple example, suppose we have $M = 2$ receivers and $N = 2$ frequencies. Then our data vector would be $X' = [X_1(\omega_1) X_1(\omega_2) X_2(\omega_1) X_2(\omega_2)]$. The general $NM \times NM$ covariance matrix would look like

$$\Sigma = \begin{bmatrix} \Sigma_{11}(11) & \Sigma_{11}(12) & \Sigma_{12}(11) & \Sigma_{12}(12) \\ \Sigma_{11}(21) & \Sigma_{11}(22) & \Sigma_{12}(21) & \Sigma_{12}(22) \\ \Sigma_{21}(11) & \Sigma_{21}(12) & \Sigma_{22}(11) & \Sigma_{22}(12) \\ \Sigma_{21}(21) & \Sigma_{21}(22) & \Sigma_{22}(21) & \Sigma_{22}(22) \end{bmatrix}$$

where the subscripts refer to vectors X_1 and X_2 , and the values in the parenthesis refer to the frequencies ω_1 and ω_2

From the above result, only those frequencies which are equal have non-zero values, so this matrix reduces to the form

$$\Sigma = \begin{bmatrix} \Sigma_{11}(11) & 0 & \Sigma_{12}(11) & 0 \\ 0 & \Sigma_{11}(22) & 0 & \Sigma_{12}(22) \\ \Sigma_{21}(11) & 0 & \Sigma_{22}(11) & 0 \\ 0 & \Sigma_{21}(22) & 0 & \Sigma_{22}(22) \end{bmatrix}$$

The inverse will have a similar form, namely

$$\Sigma^{-1} = \frac{1}{|\Sigma|} \begin{bmatrix} \sigma_{22}(11) & 0 & -\sigma_{12}(11) & 0 \\ 0 & \sigma_{22}(22) & 0 & -\sigma_{12}(22) \\ -\sigma_{21}(11) & 0 & \sigma_{11}(11) & 0 \\ 0 & -\sigma_{21}(22) & 0 & \sigma_{11}(22) \end{bmatrix}$$

with $\sigma_{ij} \propto \Sigma_{ij}$, $i, j = 1, 2$, and $|\Sigma|$ the determinant of the covariance matrix.

If we now write $A_1 = [X_1(\omega_1) X_2(\omega_1)]$ and $A_2 = [X_1(\omega_2) X_2(\omega_2)]$, then writing

$$B_1 = \begin{bmatrix} \sigma_{22}(11) & -\sigma_{12}(11) \\ -\sigma_{21}(11) & \sigma_{11}(11) \end{bmatrix}$$

and

$$B_2 = \begin{bmatrix} \sigma_{22}(22) & -\sigma_{12}(22) \\ -\sigma_{21}(22) & \sigma_{11}(22) \end{bmatrix}$$

the product $X^* \Sigma^{-1} X$ becomes $A_1^* B_1 A_1 + A_2^* B_2 A_2$.

$$\text{If we define } X(k) = \begin{bmatrix} X_1(k) \\ X_2(k) \end{bmatrix}$$

then

$$E[X^*(k) X'(k)] = E \begin{bmatrix} X_1^*(k) X_1(k) & X_1^*(k) X_2(k) \\ X_2^*(k) X_1(k) & X_2^*(k) X_2(k) \end{bmatrix}$$

and the $X^* \Sigma^{-1} X$ term in the pdf becomes, as a result of the above, the summation $\sum_{k=1}^N X^*(k) E[X^*(k) X'(k)]^{-1} X(k)$.

Note that Σ has no θ dependence, thus the determinant will not either. The sum given above will be the only term in the log likelihood to have a θ dependence, and will be the only non-zero term present when derivatives are taken.

It is now possible to find the Cramer–Rao bound on the variance of $\hat{\theta}$. In expanding out the matrix products in the above quadratic, we find that there are terms that do not

depend on the time–delay, or angle of arrival. We find that we can write the log likelihood function as

$$l(\theta) = \frac{T}{|\Sigma|} \sum_{k=1}^N S(k) [X_1^*(k)X_2(k)e^{-ik(d_1-d_2)} + X_2^*(k)X_1(k)e^{ik(d_1-d_2)}] \quad (\text{A9})$$

and therefore

$$\frac{\partial l(\theta)}{\partial \theta} = \frac{iT}{c|\Sigma|}(d_1 - d_2) \cos \theta \sum_{k=1}^N k S(k) [-X_1^*(k)X_2(k)e^{-ik(d_1-d_2)} + X_2^*(k)X_1(k)e^{ik(d_1-d_2)}] \quad (\text{A10})$$

It is straightforward to show that the expectation of this derivative is zero.

Noticing that terms in the second derivative vanish when we take the expectation, we find that the only term necessary from the second derivative is

$$\frac{\partial^2 l(\theta)}{\partial \theta^2} = -\frac{T}{c^2|\Sigma|}(d_1 - d_2)^2 \cos^2 \theta \sum_{k=1}^N k^2 S(k) [X_1^*(k)X_2(k)e^{-ik(d_1-d_2)} + X_2^*(k)X_1(k)e^{ik(d_1-d_2)}] \quad (\text{A11})$$

and the expectation of this is

$$E\left[\frac{\partial^2 l(\theta)}{\partial \theta^2}\right] = -\frac{2T^2}{c^2|\Sigma|}(d_1 - d_2)^2 \cos^2 \theta \sum_{k=1}^N k^2 S^2(k) \quad (\text{A12})$$

We also find that

$$\frac{T^2 S^2(k)}{|\Sigma|} = \frac{S^2(k)/N^2(k)}{1 + 2S(k)/N(k)} \quad (\text{A13})$$

From all of this, we find the Cramer–Rao bound on the variance of the estimate of the angle of arrival

$$\sigma_{\hat{\theta}}^2 \geq \left[\frac{2}{c^2}(d_1 - d_2)^2 \cos^2 \theta \sum_{k=1}^N k^2 \frac{S^2(k)/N^2(k)}{1 + 2S(k)/N(k)} \right]^{-1} \quad (\text{A14})$$

The general form is given by Equation (16) in [18].

This is the lower bound of the rms error of an unbiased estimator. If the actual rms error achieves this bound, we have an optimal estimator. This will not always be the case in the real world, in which case we must deal with ‘close to optimal’ estimators, or sub-optimal estimators.

Appendix B Generalised Cross Correlation Method

This is a Maximum Likelihood estimator of the time-delay between signals received at two spatially separated receivers [19, 20, 21].

The estimator is a pair of pre-filters followed by a cross correlator. The maximum of this correlator in the time domain, is the estimate of the time-delay.

If we have a signal from an unknown source, arriving at two receivers separated in space, then the received data can be written

$$\begin{aligned} x_1(t) &= s_1(t) + n_1(t) \\ x_2(t) &= \alpha s_1(t - t_d) + n_2(t) \end{aligned} \quad (\text{B1})$$

where t_d is the time-delay, signal $s_1(t)$ is uncorrelated with the noise $n_1(t)$ and $n_2(t)$, and α is attenuation.

A common method for estimating time-delay is to compute the cross correlation function (CCF),

$$R_{x_1 x_2}(\tau) = E[x_1(t) x_2(t - \tau)] \quad (\text{B2})$$

where E represents the expectation. The τ which maximises this function is the estimate of the time-delay.

As we will only have access to a finite duration signal, the LHS of Equation (B2) is also an estimate.

Via a Fourier Transform, we are able to write the CCF, $R_{x_1 x_2}(\tau)$, in terms of the cross power spectral density function (PSD) $G_{x_1 x_2}(f)$,

$$R_{x_1 x_2}(\tau) = \int_{-\infty}^{\infty} G_{x_1 x_2}(f) e^{i2\pi f \tau} df \quad (\text{B3})$$

At this point we introduce the filters, and remember that we only have an estimate of the CCF and PSD. In terms of the filtered data y_1 and y_2 , we have

$$\hat{R}_{y_1 y_2}(\tau) = \int_{-\infty}^{\infty} H_1(f) H_2^*(f) \hat{G}_{x_1 x_2}(f) e^{i2\pi f \tau} df \quad (\text{B4})$$

with $\psi(f) = H_1(f) H_2^*(f)$ being defined as a generalised frequency weighting. The weighting $\psi(f)$ may be selected to optimise certain criteria – for example, to pass signals for which the signal-to-noise ratio (SNR) is high

We use Equation (B4) to evaluate time-delay estimates.

Given our signal model from Equation (B1), we can write down the CCF (in the time domain). A Fourier Transform gives us the PSD (in the frequency domain). This is found to be the sum of the signal PSD, $G_{s_1 s_1}(f)$, multiplied by a complex exponential, and the noise PSD, $G_{n_1 n_2}(f)$. For uncorrelated noise, $G_{n_1 n_2}(f) = 0$.

A multiplication in the frequency domain may be written as a convolution in the time domain, and assuming uncorrelated noise, we have

$$R_{x_1 x_2}(\tau) = \alpha R_{x_1 x_2}(\tau) \star \delta(t - t_d) \quad (\text{B5})$$

The effect of this convolution is to spread out the peak of the CCF. A problem with this is when we have multiple time-delays. This spreading effect may cause peaks to overlap.

Therefore, the frequency weighting $\psi(f)$ is chosen to ensure large sharp peaks in the CCF. Unfortunately this leads to estimates which are sensitive to (finite time) errors, particularly at low SNR.

Let $X_i(\omega), i = 1, 2$ denote the Fourier Transform of the received data $x_i(t)$.

If the duration of the signal, T , is large compared to the absolute value of the time-delay, $|t_d|$, and the correlation time of the signal correlation function, then we are able to make use of Equation (A8), and uncouple the frequency components.

Following through, defining the vector

$$X(k) = [X_1(k) X_2(k)]' \quad (\text{B6})$$

we have the conditional pdf

$$p(X|Q) = ce^{-\frac{1}{2} \sum_{k=1}^N X^{*'}(k) Q^{-1}(2\pi k/T) X(k)} \quad (\text{B7})$$

where c is a function of the determinant of the spectral density matrix Q , which is defined to be

$$\begin{aligned} Q(k\omega_\Delta) &= T E \left[\begin{array}{cc} X_1(k) X_1^*(k) & X_1(k) X_2^*(k) \\ X_2(k) X_1^*(k) & X_2(k) X_2^*(k) \end{array} \right] \\ &= \left[\begin{array}{cc} G_{x_1 x_1}(k\omega_\Delta) & G_{x_1 x_2}(k\omega_\Delta) \\ G_{x_1 x_2}^*(k\omega_\Delta) & G_{x_2 x_2}(k\omega_\Delta) \end{array} \right] \end{aligned}$$

defining $\omega_\Delta = 2\pi/T$. For large T , $Q(k\omega_\Delta) \rightarrow Q(f)$.

The inverse is easily found, with the determinant given by

$$\begin{aligned} |Q(f)| &= G_{x_1 x_1}(f) G_{x_2 x_2}(f) - |G_{x_1 x_2}(f)|^2 \\ &= G_{x_1 x_1}(f) G_{x_2 x_2}(f) \left[1 - \frac{|G_{x_1 x_2}(f)|^2}{G_{x_1 x_1}(f) G_{x_2 x_2}(f)} \right] \end{aligned}$$

If we define a correlation coefficient

$$\gamma_{12}(f) = \frac{G_{x_1 x_2}(f)}{\sqrt{[G_{x_1 x_1}(f) G_{x_2 x_2}(f)]}} \quad (\text{B8})$$

then we have

$$|Q(f)| = G_{x_1 x_1}(f) G_{x_2 x_2}(f) (1 - |\gamma_{12}(f)|^2) \quad (\text{B9})$$

For large observation time T , we are able to replace the $X_i(k)$ with the Fourier transform $\tilde{X}_i(2\pi k/T)/T \rightarrow \tilde{X}_i(f)/T$ and the conditional pdf becomes

$$p(X|Q) = ce^{-\frac{1}{2} \int \tilde{X}^{*'}(f) Q^{-1}(f) \tilde{X}(f)} \quad (\text{B10})$$

Taking the log, and considering only those terms dependent on the parameter t_d , it can be found that the maximum likelihood estimate of t_d maximises (using the notation of [19])

$$-J_3 = 2T \int \hat{G}_{x_1 x_2}(f) \frac{1}{|G_{x_1 x_2}(f)|} \frac{|\gamma_{12}(f)|^2}{1 - |\gamma_{12}(f)|^2} e^{i2\pi f t_d} df \quad (\text{B11})$$

where

$$\hat{G}_{x_1x_2}(f) = \frac{1}{T} \tilde{X}(f) \tilde{X}^*(f) \quad (\text{B12})$$

is the estimate of the cross power spectral density function and $\gamma_{12}(f)$ is the coherence [20, 21]. In deriving the above, we make use of the relation

$$G_{x_1x_2}(f) = |G_{x_1x_2}(f)| e^{-i2\pi f t_d} \quad (\text{B13})$$

It is straight forward to derive the Cramer–Rao bound of the variance of \hat{t}_d [19].

The log likelihood function of interest, reduces to

$$l(t_d) = -\frac{J_3}{2} \quad (\text{B14})$$

Taking derivatives, and noting that $E[\hat{G}_{x_1x_2}(f)] = G_{x_1x_2}(f)$, we have the Cramer–Rao bound

$$\sigma_{\hat{t}_d} \geq \left[4\pi^2 T \int f^2 \frac{|\gamma_{12}(f)|^2}{1 - |\gamma_{12}(f)|^2} df \right]^{-1} \quad (\text{B15})$$

DISTRIBUTION LIST

Time Delay Estimation

Iain Jameson

Number of Copies

DEFENCE ORGANISATION

Task Sponsor

DNC4ISREW 1 (printed)

S&T Program

Chief Defence Scientist	1
Deputy Chief Defence Scientist Policy	1
AS Science Corporate Management	1
Director General Science Policy Development	1
Counsellor, Defence Science, London	Doc Data Sheet
Counsellor, Defence Science, Washington	Doc Data Sheet
Scientific Adviser Joint	1
Navy Scientific Adviser	1

Systems Sciences Laboratory

Chief, EWRD	Doc Data Sheet and Dist List
Research Leader, RFEW, EWRD	Doc Data Sheet and Dist List
Head, ESS, EWRD	1
Iain Jameson, EWRD	1 (printed)
Greg Noone, EWRD	1
Stephen Elton, EWRD	1
Tony Douglas, EWRD	1
John Quin, EWRD	1

DSTO Library and Archives

Library, Edinburgh	2 (printed)
Defence Archives	1 (printed)

Capability Development Group

Director General Maritime Development	Doc Data Sheet
Director General Capability and Plans	Doc Data Sheet
Assistant Secretary Investment Analysis	Doc Data Sheet
Director Capability Plans and Programming	Doc Data Sheet
Director General Australian Defence Simulation Office	Doc Data Sheet

Navy

Director General Navy Capability, Performance and Plans, Navy Headquarters	Doc Data Sheet
Director General Navy Strategic Policy and Futures, Navy Headquarters	Doc Data Sheet
Deputy Director (Operations) Maritime Operational Analysis Centre, Building 89/90, Garden Island, Sydney Deputy Director (Analysis) Maritime Operational Analysis Centre, Building 89/90, Garden Island, Sydney	Doc Data Sheet and Dist List

Army

ABCA National Standardisation Officer, Land Warfare Development Sector, Puckapunyal	Doc Data Sheet (pdf format)
SO (Science), Deployable Joint Force Headquarters (DJFHQ)(L), Enoggera QLD	Doc Data Sheet
SO (Science), Land Headquarters (LHQ), Victoria Barracks, NSW	Doc Data Sheet and Exec Summ

Air Force

SO (Science), Headquarters Air Combat Group, RAAF Base, Williamtown	Doc Data Sheet and Exec Summ
---	---------------------------------

Joint Operations Command

Director General Joint Operations	Doc Data Sheet
Chief of Staff Headquarters Joint Operation Command	Doc Data Sheet
Commandant, ADF Warfare Centre	Doc Data Sheet
Director General Strategic Logistics	Doc Data Sheet
COS Australian Defence College	Doc Data Sheet

Intelligence and Security Group

Assistant Secretary, Concepts, Capabilities and Resources	1
DGSTA, DIO	1
Manager, Information Centre, DIO	1
Director Advanced Capabilities, DIGO	Doc Data Sheet
GWEO-DDP	Doc Data Sheet

UNIVERSITIES AND COLLEGES

Australian Defence Force Academy Library	1
--	---

INTERNATIONAL DEFENCE INFORMATION CENTRES

US - Defense Technical Information Center	1
UK - DSTL Knowledge Services	1
Canada - Defence Research Directorate R&D Knowledge and Information Management (DRDKIM)	1

NZ - Defence Information Centre

1

SPARES

DSTO Edinburgh Library

5 (printed)

Total number of copies: printed 10, pdf 19

DEFENCE SCIENCE AND TECHNOLOGY ORGANISATION DOCUMENT CONTROL DATA		1. CAVEAT/PRIVACY MARKING		
2. TITLE Time Delay Estimation		3. SECURITY CLASSIFICATION Document (U) Title (U) Abstract (U)		
4. AUTHOR Iain Jameson		5. CORPORATE AUTHOR Defence Science and Technology Organisation PO Box 1500 Edinburgh, South Australia 5111, Australia		
6a. DSTO NUMBER DSTO-TR-1705	6b. AR NUMBER 013-376	6c. TYPE OF REPORT Technical Report	7. DOCUMENT DATE	
8. FILE NUMBER U 9505-25-21	9. TASK NUMBER NAV 04/281	10. SPONSOR DNC4ISREW	11. No OF PAGES 50	12. No OF REFS 24
13. URL OF ELECTRONIC VERSION http://www.dsto.defence.gov.au/corporate/ reports/DSTO-TR-1705.pdf		14. RELEASE AUTHORITY Chief, Electronic Warfare and Radar Division		
15. SECONDARY RELEASE STATEMENT OF THIS DOCUMENT <i>Approved For Public Release</i> OVERSEAS ENQUIRIES OUTSIDE STATED LIMITATIONS SHOULD BE REFERRED THROUGH DOCUMENT EXCHANGE, PO BOX 1500, EDINBURGH, SOUTH AUSTRALIA 5111				
16. DELIBERATE ANNOUNCEMENT No Limitations				
17. CITATION IN OTHER DOCUMENTS No Limitations				
18. DSTO RESEARCH LIBRARY THESAURUS Time delay estimation, Radar signals, Radar detection, Signal processing				
19. ABSTRACT We investigate the possibility of exploiting the properties of a detected Low Probability of Intercept (LPI) signal waveform to estimate time delay, and by geometry, angle of arrival. We consider the case where a highly correlated signal is received at two stationary passive receivers. The signal source is assumed stationary, and the signal waveform designed so that the ambiguity function has a sharp peak. We also restrict ourselves to low signal-to-noise ratios, namely 10 dB and less. We also examine the minimum time-delay estimate error – the Cramer–Rao bound. The results indicate that the method works well for highly correlated pulsed signals, and may prove useful for other types of signals, such as CW signals and pseudo-random noise.				